Title
Examining kinesin motor family diversity: A mechanistic study of Ncd and OSM-3 motor proteins

Author
Endres, Nicholas F

Publication Date
2006

Peer reviewed|Thesis/dissertation

Examining Kinesin Motor Family Diversity,

A Mechanistic Study of Ncd and OSM-3 Motor Proteins

by

Nicholas F. Endres

DISSERTATION

Submitted in partial satisfaction of the requirements for the degree of

DOCTOR OF PHILOSOPHY

in

Biophysics

in the

GRADUATE DIVISION

of the

UNIVERSITY OF CALIFORNIA, SAN FRANCISCO

I would like to dedicate this thesis to my family. To my parents who in addition to feeding me every Sunday, taught me to love learning and never wavered in there support and belief in me. To my sister, the other Dr. Endres, who has been an inspiration and a friend. To my late grandmother who just missed my graduation, but whose zest for life inspired me.

ACKNOWLEDGEMENTS

I would like to acknowledge my advisor Dr. Ron Vale who has supported my throughout my graduate career, through all its highs and lows. In addition to being a fabulous writer and a brilliant scientist, Ron has also been a fantastic mentor, and a good friend. It has been a pleasure to work with him.

I would like to acknowledge my collaborators without whom much of this work would not be possible. Craig Yoshioka and Dr. Ron Milligan are talented electron microscopists whose work was critical to increasing the impact of my Ncd story. They are also fun people and I enjoyed working with both of them both. I particularly appreciate Craig putting me up in his house when I came to visit San Diego. Dr. Ryan Case and Dr. Sarah Rice laid the ground work for the Ncd story without which much of this would not be possible. Uschi Weidmann, Dr. Michio Tomishige, Julia Kardon and Jeremy Epstein also were very helpful to me in the early stages of the Ncd project development. Dr. Miki Imanishi began the OSM-3 project and was kind and gracious enough to let me take a leadership role in finishing the project. Dr. Arne Gennerich is fantastic with the optical trap and has been a pleasure to work with. His experiments, added in the last few weeks before submission really helped to shore up our hypothesis about the regulation of OSM-3. Arne also graciously conformed to my rushed schedule for graduation even though he had other projects going on. Discussions with Guangshou Ou, Xiaoyu Pan, and Dr. John Scholey were invaluable for putting the OSM-3 story in a biological context. They generously shared some of their unpublished data with me which was an important part of our OSM-3 paper, and they

included me as a collaborator on a project examining the mechanical competition betwen OSM-3 and Kinesin-II.

I would like to thank all of the members of the Vale Lab with whom I have had the pleasure to work with. Although I can't name everyone here, there isn't a single person in the lab who hasn't taught me something, or helped me through some bind. I would like to especially thank the lab managers Nora Bom-Homer, Uschi Weidmann, and Nan Zhang who kept the ship afloat, bailed me out of some jams and were also really nice people. I would like to thank Phoebe Grigg for all the wonderful things she has done for the Vale Lab, and for her fantastic help with finishing this thesis. The Vale Lab was an incredible atmosphere for exciting and collaborative science in my time here, and I think that is a testament not only to Ron but to all the people who worked here.

I would also like to acknowledge some of the others that were instrumental in my career. Although we never quite finished any of our collaborations, the Cooke Lab helped me to learn the nuts and bolts of working with kinesin and tubulin, and were fun to work with. Dr. Roger Cooke was always very supportive of me and gave me great advice throughout my career sitting both on my orals and thesis committees. Jonathan Weissman also served on my thesis committee and was a pleasure to work with. Finally, although I will not be discussing it in this thesis, I would like to thank Dr. Charles Craik, Dr. Kinkead Reiling, Dr. Bob Stroud and Dr. Deb Dauber for the completion of a wonderful project on HIV protease that I was lucky enough to be a part of. Dr. Charles Craik took me in as a high school SEP student and has been a long time booster and mentor

I would also like to acknowledge some of the larger community of UCSF. Our neighbors the Mullins and Walter Labs were full of great people who were always generous in sharing their equipment and their time. The Biophysics Program was a fantanstic environment for learning full of brilliant and generous professors, and fantastic students. I would especially like to thank Julie Ransom for being a great person to talk to and for her tireless defense and maintenance of the Biophysics Program. In general I would like to the powers that be at UCSF for maintaining a fantastic and unique culture for doing collaborative science.

Finally I would like to thank my friends both in and out of UCSF for providing me with a sense of perspective and making my years here in San Francisco a pleasure, my girlfriend Melinda Wallace for making my world a little bit brighter, and my loving family to whom I have dedicated this thesis.

Examining Kinesin Motor Family Diversity,

A Mechanistic Study Of Ncd And OSM-3 Motor Proteins

by

Nicholas F. Endres

ABSTRACT

Kinesin motor proteins produce motion and force along microtubules and are essential for the organization of subcellular components (Vale, 2003). The kinesin superfamily is divided into 14 subfamilies that carry out a variety of biological functions (Miki et al., 2005). In spite of their diversity, Kinesin motors all share a conserved catalytic domain that binds to microtubule and hydrolyzes ATP (Vale and Milligan, 2000). The two studies presented here are examples of how kinesin motors can be uniquely adapted to perform their specific cellular functions. The first study focuses on the Kinesin-14 family member Ncd. Most kinesin motors, exemplified by Kinesin-1, move towards the microtubule plus end, and the structural changes that govern this directional preference have been described (Rice et al., 1999). In contrast, the structural changes underlying the minus-end-directed motility of Kinesin-14 motors are less well understood. Using cryo-electron microscopy, we demonstrate that a coiled-coil mechanical element of microtubule-bound Ncd rotates ~70° towards the minus end upon ATP binding. Extending or shortening this coiled coil increases or decreases velocity, respectively, without affecting ATPase activity. Our results show that the force-producing conformational change in Ncd occurs on ATP binding, as in other kinesins, but involves the swing of a lever-arm mechanical element

similar to that described for myosins. The second study focuses on OSM-3, a Kinesin-2 family member involved in intraflagellar transport (IFT) (Scholey et al., 2004). Here, using a single molecule fluorescence assay, we show that bacterially-expressed OSM-3 GFP does not move processively (multiple steps along a microtubule without dissociation). However, a single point mutation in a predicted hinge region of the OSM-3 coiled-coil stalk, as well as a deletion of that hinge, activates robust processive movement of OSM-3. The processivity of wild-type OSM-3 also can be activated by attaching the motor to beads in an optical trap. Sucrose gradient analysis reveals that OSM-3 adopts a compact conformation that becomes extended in the hinge mutants or at high salt. We propose that the processivity of OSM-3 is repressed by an intramolecular interaction in vivo that can be relieved by IFT cargo binding.

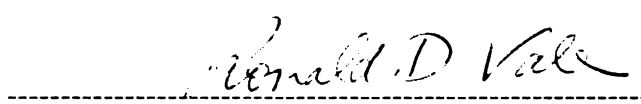

Ronald D. Vale, Ph.D.

Advisor and Chairperson

TABLE OF CONTENTS

LIST OF TABLES

LIST OF FIGURES

Cell survival, differentiation and function depend on the precise spatial organization of cellular organelles, signaling proteins, cytoskeletal elements and genetic material. Motor proteins, which utilize the chemical energy stored in ATP to produce motion along and to modulate the stability of cytoskeletal elements, are crucial for maintaining spatial organization of subcellular components. Kinesin motor proteins, one of three superfamilies of motor proteins, interact with microtubules and play a crucial role in this subcellular organization (Vale, 2003). Kinesins transport a wide variety of cargo including ER, golgi, endosomes, lysosomes, mitochondria and transport vesicles along microtubule filaments (Kamal and Goldstein, 2002). This kinesin-driven transport, although no doubt important in many cellular contexts (Vale, 2003), is essential for survival neuronal cells (Guzik and Goldstein, 2004), and defects in transport can be linked to several neurodegenerative disorders (Gunawardena and Goldstein, 2004; Mandelkow and Mandelkow, 2002). In addition to their crucial role in vesicular transport, kinesin proteins also play a crucial role in organizing the cytoskeleton, including the formation and maintenance of cilia (Scholey, 2003) and cell division (Heald, 2000).

The diversity of cellular functions for kinesin is paralleled by the diversity of the kinesin superfamily which can be subdivided into 14 distinct subfamilies (Miki et al., 2005). There are 45 different kinesins in the mouse and human genomes of which 38 are detectably expressed in mouse brain tissue, implying that diversity of Kinesin function is important for normal neuronal function (Miki 99). However exactly how this diversity in sequence is

translated into functional diversity is poorly understood. Although the topology of these kinesins vary, they all share a highly conserved catalytic domain which binds to microtubules and hydrolyzes ATP (commonly referred to as the motor domain) (Vale and Milligan, 2000). The central question of my research was to determine how the Kinesin family can use a common motor domain to perform diverse functions. The two studies presented here are examples of how kinesin motors can be uniquely adapted to perform their specific cellular functions.

How does the Kinesin-14 family of proteins support minus-end directed movement of microtubules?

Part of the diversity of the kinesin family has to do with how the motor converts ATP binding into mechanical force and movement. Although most kinesins move towards the plus-end of the microtubule (Miki et al., 2005), members of the Kinesin-14 family move in the opposite direction (Endow et al., 1990; Endow et al., 1994; McDonald et al., 1990), and members of two families of motor proteins participate in the destabilization of microtubules (Hunter et al., 2003; Wordeman and Mitchison, 1995). This diversity of function is accomplished despite considerable conservation in the core motor domain.

The Kinesin-14 family member Ncd is the focus of the first chapter of my thesis. Ncd plays a critical role in mitosis, since cells lacking Ncd have defects in spindle formation and chromosome segregation (Endow et al., 1990; Goshima and Vale, 2003). In addition to its kinesin motor domain, Ncd also has a tail domain which binds to microtubules in an ATP

independent manner and allows Ncd to act as a microtubule cross linker (Karabay and Walker, 1999; Wendt et al., 2003). The role that Ncd plays in mitosis is believed to be due to its ability to cross-link microtubules and to generate a poleward force opposite to that of the plus-end directed crosslinking motor Kinesin-5 (Sharp et al., 1999b).

Unlike motors in the well studied Kinesin-1 family which move towards the plus-end of the microtubule processively (taking several steps before dissociating from the microtubule), Ncd produces non processive movement towards the minus-end of the microtubule (deCastro et al., 2000; McDonald et al., 1990). I was interested in determining how the Kinesin-14 family member Ncd utilizes a motor domain highly similar to that of Kinesin-1 (43% identity, (Sablin et al., 1996)) to move in the opposite direction.

Because its motor domain is so similar, one would expect that the mechanism for Ncd motility although opposite in direction, should share some features with the mechanism of the plus-end directed Kinesin-1, the best understood of the kinesin families. Both Kinesin-1 and Ncd form a dimer through a coiled-coil domain referred to as the neck domain (Kozielski et al., 1997; Sablin et al., 1998). The motion of Kinesin-1 is driven by the alternating catalysis of the two motor domains, which move along the microtubule in a hand-over-hand manner (Hackney, 1994; Yildiz et al., 2004). In order for Kinesin-1 to move along microtubules, the motor domains must be associated and dissociated from the microtubule at different steps in the ATP hydrolysis cycle. This is accomplished by a relationship between the state of the nucleotide bound to the motor domain and the affinity of the motor domain for the microtubule (Crevel et al., 1996; Romberg and Vale, 1993). The directionality of

Kinesin-1 is determined by the motion of its neck linker (a structural element connecting the motor domain to the neck coiled-coil) which changes conformation in response to nucleotide (Rice et al., 1999). The processivity of the Kinesin-1 motor requires a kinetic coordination of the ATP hydrolysis cycles of the two motor domains (Hackney, 1994; Ma and Taylor, 1997; Rosenfeld et al., 2003), and a proper geometry between these domains which allows for two motor heads to be associated with the microtubule (Romberg et al., 1998; Tomishige and Vale, 2000).

Since the strong and weak microtubule binding states of Ncd were shown early on to be identical to Kinesin-1 (Crevel et al., 1996), it was suspected that the critical differences between Ncd and Kinesin-1 were likely to be in the mechanical element, and/or the geometry of the dimer. When I began my research with Ncd it was clear that its neck coiled-coil was the directional determinant. This was best shown in a series of experiments with chimeras of Ncd and Kinesin-1, in which the directionality of Kinesin-1 could be reversed by fusing its motor domain to the neck coiled-coil of Ncd (Endow and Waligora, 1998). Unlike the neck coiled-coil of Kinesin-1 which is connected to the motor core through a short beta strand termed the neck linker, the neck coiled-coil of Ncd is a continuous coiled-coil which is attached directly to the motor (Sablin et al., 1998). The geometry of the two heads of the Ncd dimer also differ from Kinesin-1. 3-D reconstructions of electron micrographs of Ncd bound to the microtubule show that the two motor domains line up perpendicular to the long axis of the microtubule with only one motor domain bound to the microtubule in several different nucleotide states (Hirose et al., 1998). This geometry between the Ncd motor

domains is not optimal for long range processive movement which would required motor domains to lines up parallel to the microtubule axis.

When I began my research, it was widely believed that a conformational change in the neck region of Ncd was responsible for the minus-end -directed motility of the motor. However, the precise nature and timing of that structural change was unknown. Some important clues came from the docking of the Ncd crystal structure (solved in its solution ADP bound state) to electron micrographs of the Ncd monomer bound to microtubules (Sablin et al., 1998). This docking suggested that the neck coiled-coil faces towards the plus-end of the microtubule upon binding of the motor to the microtubule and release of ATP. Subsequent electron micrographs of the Ncd dimer were consistent with this model (Hirose et al., 1998; Sosa et al., 1997). Based on these docking it was proposed that a change in the position of the Ncd neck towards the minus-end of the microtubule could be responsible for the motility of the motor (Sablin et al., 1998). Electron micrographs of Ncd with an SH3 domain fused its N-terminus as a density marker (Wendt et al., 2002) and a crystal structure of an ATP hydrolysis-deficient point mutant of Ncd (Yun et al., 2003) provided evidence, albeit indirect, that the Ncd neck could have an alternate conformation. However these studies failed to reveal the exact nature and timing of this conformational change and led to the proposal of two conflicting models for Ncd motility. Both of these studies pointed towards a mechanism for Ncd motility in which a conformational change in the neck acts as a lever arm to generate a minus-end-directed power stroke in a manner similar to Myosin II (Suzuki et al., 1998; Uyeda et al., 1996). The first chapter of this thesis discusses the experiments I designed to test this hypothesis.

How does the Kinesin-2 motor family differ from Kinesin-1?

While the difference in function between the Kinesin-14 subfamily and other Kinesin families is very clear, the differences among the 11 Kinesin subfamilies that all move towards the plus-end of the microtubule is much less clear. In the second part of my thesis, I examine the mechanism of one of these plus-end motors, OSM-3.

OSM-3 is a Kinesin-2 family member from *Caenorhabditis elegans* which is essential for the construction and maintenance of sensory cilia in chemosensory neurons (Cole et al., 1998; Perkins et al., 1986; Shakir et al., 1993; Snow et al., 2004). OSM-3 cooperates with another kinesin-2 family member (the heterodtrimeric protein Kinesin-II (Cole et al., 1993)) in the intraflagellar transport of particles containing structural and signalling proteins (IFT particles) (Snow et al., 2004). Both motors cooperate to move IFT's along the 'middle segment' of the cilia consisting of double microtubules, while only Osm-3 transports IFT's along the 'distal segment' consisting of single microtubules (Snow et al., 2004). OSM-3 IFT particles have been observed moving at a velocity of 1.3 μm/s along the distal segments of these cilia, and along both segments of the cilia in animals which have Kinesin-II knocked out (Snow et al., 2004); however, the motility of OSM-3 has not been characterized in vitro. We show here, using single molecule fluorescence assay, that bacterially-expressed OSM-3 GFP does not move processively along microtubules.

This lack of processivity for OSM-3 was unexpected for a motor that was known to involved in long-range transport. The second chapter of this thesis, I discuss our attempts to

characterize the motility of OSM-3 with the goal of determining the structural determinants for its lack of processivity compared to the Kinesin-1. We discovered that the processivity of OSM-3 was regulated by a novel intramolecular interaction in vitro, and could be regulated by cargo binding in vivo.

CHAPTER 1

A lever-arm rotation drives motility of the minus-end-directed kinesin Ncd

The work presented in Chapter 1 is the result of a collaboration between myself, Craig Yoshioka, and Dr. Ron Milligan. I designed and prepared all of the constructs used in the study and conducted all of the biochemical experiments. Craig Yoshioka, in Dr. Milligan's lab, conducted the cryo-electron microscopy experiments.

This chapter is reprinted from Nature with permission. Originally published as:

A lever-arm rotation drives motility of the minus-end-directed kinesin Ncd.

Endres NF, Yoshioka C, Milligan RA, Vale RD.

Nature. 2006 Feb 16;439(7078):875-8. Epub 2005 Dec 28.

SUMMARY

Kinesins are microtubule-based motor proteins that power intracellular transport (Hirokawa and Takemura, 2004; Sharp et al., 2000). Most kinesin motors, exemplified by Kinesin-1, move towards the microtubule plus end, and the structural changes that govern this directional preference have been described (Asbury et al., 2003; Rice et al., 1999; Yildiz et al., 2004). By contrast, the nature and timing of the structural changes underlying the minus-end-directed motility of Kinesin-14 motors (such as *Drosophila* Ncd (Endow et al., 1990; McDonald et al., 1990)) are less well understood. Using cryo-electron microscopy, we demonstrate that a coiled-coil mechanical element of microtubule-bound Ncd rotates ~70° towards the minus end upon ATP binding. Extending or shortening this coiled coil increases or decreases velocity, respectively, without affecting ATPase activity. An unusual Ncd mutant that lacks directional preference (Endow and Higuchi, 2000) shows unstable nucleotide-dependent conformations of its coiled coil, underscoring the role of this mechanical element in motility. These results show that the force-producing conformational change in Ncd occurs on ATP binding, as in other kinesins, but involves the swing of a lever-arm mechanical element similar to that described for myosins.

INTRODUCTION

Crystal structures of the Ncd dimer show a coiled coil extending directly from the pair of catalytic cores in dimeric Ncd (termed the 'neck') (Kozielski et al., 1999; Sablin et al., 1998; Yun et al., 2003), and mutagenesis experiments indicate that the proximal portion of the neck functions as the mechanical element that powers minus-end-directed motility (Endow and Waligora, 1998; Sablin et al., 1998). Previous cryo-electron microscopy (cryo-EM) studies of dimeric Ncd suggested that the neck extends towards the microtubule plus end in the nucleotide-free, microtubule-bound complex. This assignment was based on the position of an amino-terminal Src homology domain 3 (SH3) domain used as a marker for the neck, because the neck itself was not visible in this study (Wendt et al., 2002). Neither the neck nor the SH3 marker was observed in the presence of AMPPNP, however, which led to the proposal that ATP binding causes the Ncd neck to transition into a detached and freely diffusing state and that the shift in the average position of this freely rotating neck towards the microtubule minus end is the driving force for Ncd motility. A conflicting model of the nature and timing of the power stroke has been proposed on the basis of the crystal structure of a motility-deficient Ncd point mutant (NcdN600K) (Yun et al., 2003), which shows the neck in a different orientation that is predicted to point towards the microtubule minus end. It has been proposed that this structure represents the nucleotide-free state of the motor and that a minus-end-directed power stroke occurs on release of ADP. Thus, the exact nature and timing of the motility-producing conformational change in Ncd remains uncertain.

RESULTS

Here we have used cryo-EM to investigate the position of the neck in dimeric Ncd (residues 281–700; see Methods) bound to a microtubule in the absence of nucleotide and in the presence of two mimics of an ATP-like state, AMPPNP (a non-hydrolysable ATP analogue) and ADP-AlF_4^- (a transition-state analogue). Helical image analysis of 15 protofilament microtubules was used to calculate three-dimensional (3D) density maps (Fig. 1a–c and Methods). All three maps show two distinct globular domains of similar size and shape, which represent the two heads of the Ncd dimer. As seen before (Arnal et al., 1996; Hirose et al., 1996; Sosa et al., 1997), only one of the two Ncd heads interacts with the microtubule. In the nucleotide-free state, an elongated density emerges from between the two heads of the Ncd dimer, and its length (~65 Å) matches the expected length of the portion of the Ncd coiled coil that emerges beyond the motor domain. This same elongate density was observed in constructs with two different N-terminal tags (SH3 domain, Fig. 1; or His_6, Supplementary Fig. 1), indicating that the density was not an artefact created by a particular tag. In contrast to the previous cryo-EM study, which did not visualize the neck directly (Wendt et al., 2002) and has been subject to re-interpretation (Yun et al., 2003), the clear connection of the neck density to the Ncd heads in our maps allows us to conclude unambiguously that the Ncd neck is pointing towards the plus end of the microtubule in the nucleotide-free state.

Our cryo-EM maps show a markedly different conformation of the Ncd motor in the presence of ATP analogues. With AMPPNP, the neck and unbound head of Ncd are rotated

by ~70° towards the minus end of the microtubule relative to their positions in the nucleotide-free state, whereas the position of the bound head remains unchanged (Fig. 1b; see Supplementary Fig. 2 for difference maps). The neck density is slightly weak, which may reflect either the data quality or some conformational flexibility, but it can be clearly observed projecting from the two heads of the dimer. In the ADP-AlF_4^- map, the neck density is stronger and better defined (Fig. 1c). Despite these variations, an overlay of the two maps shows that the orientation of the heads and neck are identical in the AMPPNP and ADP-AlF_4^- states (Supplementary Fig. 2). Thus, our data indicate that the Ncd neck has a preferred minus-end-pointing position in the ATP-like states and is not completely random in the ATP-like states of the cycle as has been suggested (Wendt et al., 2002). These results indicate that ATP binding causes a ~70° rotation of the neck and unbound head toward the minus end of the microtubule.

We next used a docking approach to examine the relationship between the two microtubule-bound states of Ncd observed here and the two published X-rays structure of the Ncd dimer (Sablin et al., 1998; Yun et al., 2003). We obtained an excellent fit of the wild-type Ncd/ADP crystal structure into the cryo-EM maps of the nucleotide-free state (Fig. 1d). In particular, the neck of the Ncd/ADP structure occupies the elongated density extending from the two catalytic cores (Fig. 1d), and the known microtubule-binding elements in the bound head are positioned in close proximity to tubulin (Sosa et al., 1997; Woehlke et al., 1997) (Supplementary Fig. 3). Keeping the bound head in the same orientation on the microtubule, we docked the crystal structure of the Ncd mutant N600K (NcdN600K) (Yun et al., 2003) into the maps of the Ncd-microtubule complex in the ADP-AlF_4^- state. This

structure fitted reasonably well (Fig. 1e), but was improved by a ~10° rigid-body rotation of the neck and unbound head in the NcdN600K structure (Fig. 1f). Although this slight difference suggests that the crystal structure of this non-motile Ncd mutant in solution might not be a perfect representation of the conformation of the wild-type motor bound to microtubules, our results argue that the NcdN600K structure closely approximates the microtubule-bound ATP state, rather than the nucleotide-free state as previously suggested (Yun et al., 2003).

Having successfully visualized nucleotide-mediated conformational changes in wild-type Ncd, we examined an Ncd point mutant N340K (NcdN340K) that can generate motion towards either the plus end or the minus end of microtubules with roughly equal probability (Endow and Higuchi, 2000). Because the structural basis of such bidirectional transport remains unresolved, we examined the NcdN340K–microtubule complex in different nucleotide states. In the density maps of NcdN340K in its nucleotide-free state (Fig. 1g), the shape of the unbound head is not as well defined as it is in the maps of the wild-type motor, and an elongated neck density is not observed. However, an additional disconnected density is observed at the position occupied by the N-terminal end of the neck in the wild-type motor (highlighted in Fig. 1g). One possible interpretation of this density is that the neck and unbound head in the mutant Ncd dimer occupy both the pre-stroke and post-stroke positions in the nucleotide-free state and that the 3D map reflects an average of these two positions. Consistent with this notion, averaging the wild-type nucleotide-free and ADP-AlF_4^- maps yielded a less well-defined unbound head and a disconnected neck density, similar to that seen in the NcdN340K nucleotide-free map (Fig. 1i).

In the NcdN340K/AMPPNP (Supplementary Fig. 4) and NcdN340K/ADP-AlF_4^- (Fig. 1h) maps, the neck density is completely absent, indicating an unstable neck position, and the detached head is also poorly defined (comparisons of NcdN340K/ADP-AlF_4^- and NcdN340K/AMPPNP maps show no significant differences; Supplementary Fig. 4). These data suggest a possible model of the bidirectional motion in which the mutant motor begins its ATPase cycle by binding to a microtubule with its neck oriented either towards the minus end or the plus end, and then adopts a conformationally averaged midpoint position after ATP binding. In this model, the initial direction of movement would be stochastically determined, but once motion begins in a particular direction it could continue in the same direction by virtue of cooperative effects of an ensemble of motors.

Our cryo-EM experiments suggest that Ncd uses its neck as a lever arm to generate a minus-end-directed power stroke in a manner similar to the rotation of the light-chain-binding domain in myosin II. For a lever-arm mechanism, the velocity of the motor should be proportional to the length of its lever arm (Uyeda et al., 1996). Consistent with this prediction, a series of successive neck truncations caused a progressive decrease in velocity in a microtubule-gliding assay, but did not affect enzymatic turnover (ATPase catalytic rate constant, k_{cat}; Fig. 2a). This finding is consistent with previous work on Ncd truncations (Stewart et al., 1993; Yun et al., 2003), although ATPase activity was not examined in those studies. Truncation experiments are difficult to interpret, however, because the loss of protein structure could damage motor function in unanticipated ways. We therefore sought to increase velocity by extending the length of the neck with a four-heptad leucine zipper coiled-coil motif ('LZ extension'). As expected for a lever-arm model, fusion of this LZ

extension to the native Ncd neck at three different positions increased microtubule gliding velocity without changing ATPase k_{cat} (Fig. 2a). This increase in velocity was not observed when a flexible glycine-serine linker was inserted between the LZ extension and the native Ncd neck (Fig. 2a), suggesting that the LZ extension increases Ncd velocity by extending the length of the mechanical element and not by some other mechanism. The compiled velocity data from the seven truncated or extended neck constructs show that microtubule gliding velocity is proportional to the predicted length of the neck, regardless of whether native or nonnative (LZ extension) residues were used, but ATPase k_{cat} remains unaffected (Fig. 2b, c). Taken together, these data support the notion that a lever-arm rotation of the Ncd neck powers minus-end-directed motility.

A model of Ncd motility evoking the rotation of the neck suggests that the unbound head may not be necessary to generate motility. To test this notion, we prepared a single-headed Ncd heterodimer (N280_Het; Fig. 2a) in which one polypeptide consisted of an intact Ncd catalytic core and neck (residues 280–700) and the second polypeptide consisted of the neck region alone (residues 281–347; Supplementary Fig. 5a and Methods). This motor elicited microtubule gliding at a velocity comparable to that of the normal two-headed Ncd homodimer with a similar ATPase k_{cat} (Fig. 2a). Thus, although our cryo-EM data show that the unbound head rotates along with the neck, the functional data from the heterodimer indicate that contacts between the neck and unbound head are not essential for the mechanism and that the neck alone is sufficient to act as a lever arm.

Studies have also shown that a naturally occurring Kinesin-14 heterodimer in yeast (the Kar3p–Cik1p complex, a motor polypeptide in complex with a motor-less coiled coil (Barrett et al., 2000)) is an active, force-producing motor (Chu et al., 2005; Sproul et al., 2005). To determine whether the lever-arm motion of the Ncd neck requires a stable coiled-coil interaction, we also tested the motility of an Ncd monomer construct (N325). This construct showed >25-fold reduced motility compared with the single-headed heterodimer, but had an ATPase activity similar to that of the other constructs (Fig. 2a and Supplementary Fig. 5). Thus, a stable coiled coil is required for optimal function of the motor, as would be expected for a lever-arm model.

On the basis of our structural and functional data, we propose the following model of Ncd motility (Fig. 3). Ncd from solution binds to microtubules using one of its heads, triggering ADP release (Lockhart and Cross, 1994). The excellent fit of the Ncd/ADP structure to the nucleotide-free maps suggests that microtubule binding and ADP release do not produce large-scale conformational changes in the Ncd dimer. Our cryo-EM data suggest that ATP binding leads to a ~70° rigid-body rotation of the neck that produces a minus-end-directed displacement. A subsequent protein isomerization step, possibly before phosphate release, triggers the formation of a weakly bound state and the dissociation of Ncd from the microtubule (Foster et al., 1998; Pechatnikova and Taylor, 1997). The neck lever arm can then return to its pre-power stroke position after dissociating from the microtubule, thereby completing the cycle (Fig. 3). Although this overall scheme is supported by our data, questions remain open about the proposed lever-arm mechanism. Specifically, although our data unequivocally show a preferred position of the lever arm in the AMPPNP and ADP-

AlF_4^- states, the weaker density in our AMPPNP maps suggests that this post-powerstroke state may not be completely rigid and fixed in position, as envisaged by classical swinging crossbridge models of myosin. Future work on this issue will require dynamic measurement of the lever-arm position in different nucleotide states with high spatial and temporal resolution.

Our work shows that the mechanical event in the minus-end-directed Ncd (rotation of the coiled-coil neck) is coupled to the same step of the ATPase cycle (ATP binding) as the mechanical event in the plus-end-directed kinesins (neck linker docking). Thus, reversal of direction in Kinesin-14 motors is accomplished by the evolution of a unique mechanical element that can take advantage of existing conformational changes in the catalytic core, as is also true for direction reversal by the myosin VI motor (Menetrey et al., 2005). Unlike conventional kinesin, which is built for long-distance processive movement, Ncd is a nonprocessive motor (deCastro et al., 2000; Pechatnikova and Taylor, 1999) designed for microtubule crossbridging and tension development in meiotic or mitotic spindles (Sharp et al., 1999b). In this regard, the functions of Ncd are more similar to the tension-generating myosin II motors in muscle. Thus, Ncd and muscle myosin convergently evolved a similar strategy for motility involving a large-scale rotation of an elongated lever and the primary use of only one of the two heads in the motor dimer.

METHODS

Cloning and protein preparation

The constructs used for motility and ATPase assays had an N-terminal pET104 BioEase tag (Invitrogen) for biotinylation and the cryo-EM constructs had an N-terminal SH3 domain cloned from human Nck1 fused to residue 281 of Ncd. All constructs had an N-terminal His_6 tag for purification. The LZ extensions (Fig. 2) contained the yeast GCN4 sequence (VKQLEDKVEELLSKNYHLENEVARLKKLV), and N280_LZ_GS contained a glycine-serine linker (GGGSGGGSGGGS). N280_Het was prepared by coexpressing a biotin- and His_6-tagged neck domain (281–347) with an untagged motor domain (280–700) on the same pET-17b plasmid (Invitrogen) using a single T7 promoter. Proteins were expressed and purified from a Ni^{2+}-NTA agarose column (Qiagen) as described (Case et al., 1997). For motility and ATPase assays, a microtubule affinity purification step, similar to that reported previously (Case et al., 1997), was used to select for active motors. N280_Het required an additional gel filtration purification step (Supplementary Fig. 5).

Cryo-EM and helical image analysis

Ncd (4–7 mg ml^{-1}) was dialysed against 25 mM MOPS (pH 7.25), 100 mM NaCl, 2 mM $MgCl_2$, 1 mM EGTA and 1 mM dithiothreitol and was centrifuged (100,000*g*, 15 min) to remove any precipitate. Frozen grids containing microtubules (5 mg ml^{-1}) and Ncd were prepared as described (Sosa et al., 1997) with a final concentration of nucleotide of 5 mM or 1 U of apyrase. Imaging and image analysis were carried out essentially as described (Sosa et

al., 1997), with an FEI CM200FEG electron microscope and Gatan cold stage. The number of data sets averaged and the total number of asymmetric units contributing to each 3D map were as follows: Ncd/AMPPNP, 20 data sets, 17,600 particles; Ncd/nucleotide-free, 24 data sets, 17,100 particles; Ncd/ADP-AlF_4^-, 26 data sets, 23,700 particles; Ncd(N340K)/AMPPNP, 20 data sets, 12,150 particles; Ncd(N340K)/AlF_4, 20 data sets, 13,000 particles; Ncd(N340K)/nucleotide-free, 29 data sets, 17,250 particles. For the figures, all 3D data sets were fitted and scaled to a reference created by averaging the microtubule–Ncd/AlF_4^- and microtubule–Ncd/nucleotide-free data (Fig. 1h).

Microtubule gliding and ATPase assays

For gliding assays, glass slides were treated with 0.5 mg ml^{-1} of biotinylated bovine serum albumin (Pierce) and then 0.5 mg ml^{-1} of streptavidin (Pierce) before the motor (200–400 nM for homodimers, 2 mM for heterodimer) was added. Gliding velocities of rhodamine-labelled microtubules were measured as described (Case et al., 1997) in motor buffer (25 mM MOPS, 100 mM NaCl, 1 mM EGTA, 2 mM $MgCl_2$ and 5% sucrose; pH 7). ATP hydrolysis rates were measured by an Enzchek assay kit (Molecular Probes) using 10–40 nm of motor and 0–50 mM microtubules in motor buffer with 10 mM paclitaxel and NaCl reduced to 25 mM. Hydrolysis of ATP was plotted against microtubule concentrations, and data were fitted to a Michaelis–Menton equation to determine k_{cat}.

FIGURES

Figure 1: 3D maps of Ncd–microtubule complexes by cryo-EM. a–c, Wild-type Ncd in the absence of nucleotide (**a**) and in the presence of the nucleotide analogues Mg^{2+}-AMPPNP (5 mM, **b**) and Mg^{2+}-ADP-AlF_4^- (5 mM, **c**). Putative density for the bound head, unbound head and neck region are marked as H_B, H_U and N, respectively. Arrows indicate the rotation of the unbound head and neck between the nucleotide-free and ATP-like states. **d–f**, Ncd crystal structures docked onto wild-type maps. Shown is the Ncd-ADP structure (Sablin et al., 1998) docked onto the nucleotide-free maps (**d**). The NcdN600K structure (Yun et al., 2003) (**e**), the NcdN600K structure with a 10° rotation of the unbound head and neck about Gly 347 (the residue marking the boundary between the neck and the catalytic core) (**f**), are shown docked to the Mg^{2+}-ADP-AlF_4^- maps. **g**, **h**, Cryo-EM maps for the bidirectional mutant NcdN340K, without nucleotide (**g**) and with 5 mM Mg^{2+}-ADP-AlF_4^- (**h**). 5 mM Mg^{2+}-AMPPNP produces an equivalent map to 5 mM Mg^{2+}-ADP-AlF_4^- (Supplementary Fig. 3). **i**, Density map generated by averaging the Ncd wild-type nucleotide-free and Mg^{2+}-ADP-AlF_4^- data. Detached density in NcdN340K nucleotide-free map (**g**) and in Ncd average map (**i**) circled in red. All figures are oriented so that the plus end of the microtubule axis is at the top of the page. Figures were generated with Pymol (Delano Scientific).

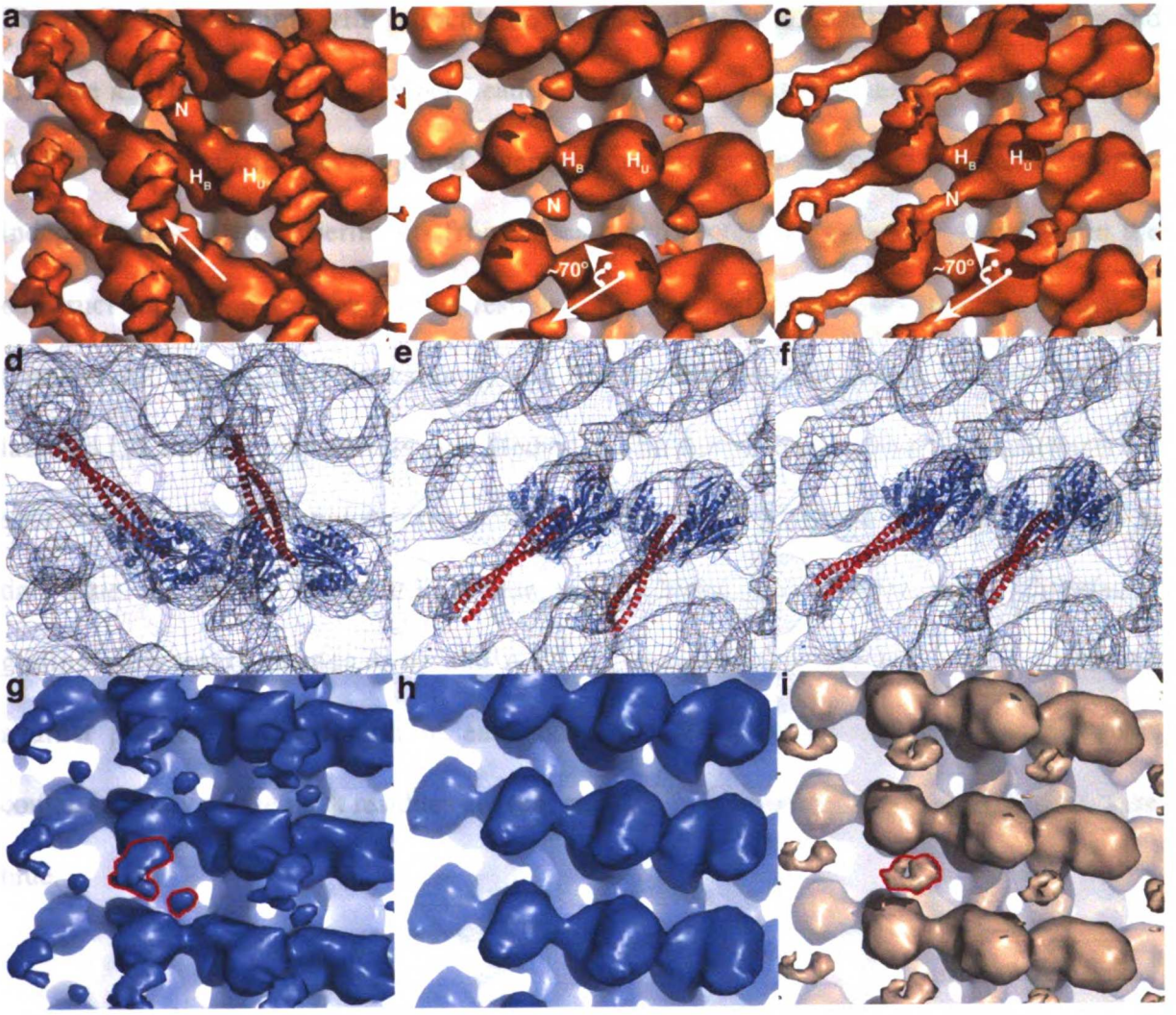
a
N
H_B
H_U
b
H_B
H_U
N
~70°
c
H_B
H_U
N
~70°
d
e
f
g
h
i

Figure 2: Ncd mutants with truncated or extended necks. a, Gliding assay velocities and ATPase k_{cat} (in ATP molecules per head per s). Velocity data are the mean±s.d. (n>150); ATPase k_{cat} data are the weighted average and errors obtained from the fits of two independent ATPase experiments from at least two protein preparations. Numbers in the construct name represent the starting residue for the native Ncd residues in the construct. N-terminal LZ extensions (29 residues) and the flexible Gly-Ser linker (12 residues) are labelled LZ and GS, respectively (see Methods). The domain structures of the constructs are shown on the left with motor cores in black, native neck residues in red, LZ extensions in dark blue, the flexible linker in light blue, and the biotin tag in orange. **b, c**, Velocities of gliding movement (mean±s.d; **b**) and ATP k_{cat} (weighted average and errors; **c**) plotted against predicted neck length of each construct. Data points representing constructs containing only native neck residues are red, and data from constructs with LZ extensions are blue.

A.

Ncd Neck Constructs	Gliding Velocity (nm/s)	ATP Turnover (ATP/head/s)
N236	150 ± 20	3.3 ± 0.5
N280_LZ	140 ± 22	4.0 ± 0.7
N308_LZ	110 ± 18	4.5 ± 0.7
N281	97 ± 15	4.6 ± 0.6
N322_LZ	82 ± 20	4.3 ± 0.6
N308	53 ± 12	4.3 ± 0.6
N322	52 ± 12	4.2 ± 0.8
N325	4 ± 3	3.8 ± 0.8
N280_GS_LZ	101 ± 16	5.6 ± 0.9
N280_Het	97 ± 18	4.8 ± 1.0

B.

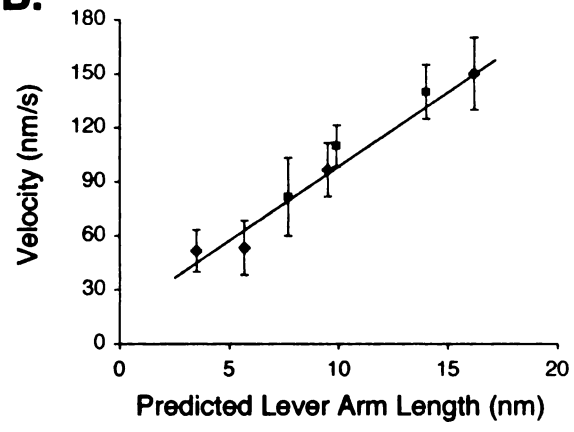

C.

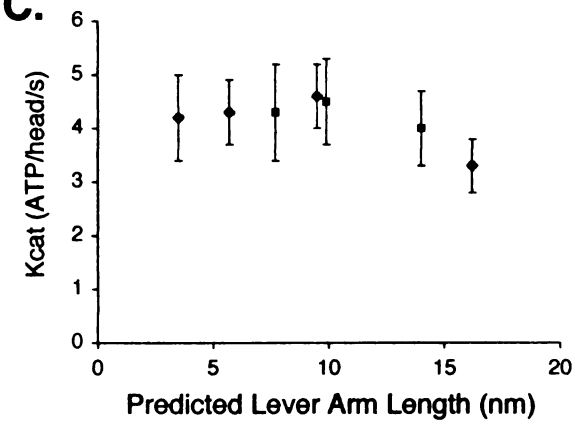

Figure 3: Model of the Ncd motility cycle. The model is based on surface representations of the docked Ncd structures (Fig. 1d, f). The microtubule is oriented so that the plus end is on the right. In this model, ATP binding causes a rotation of the neck (coloured red in the nucleotide-free and yellow in the ATP state) that leads to a minus-end displacement along the microtubule (indicated by the red arrow). After this lever-arm rotation, the motor releases from the microtubule after nucleotide hydrolysis but probably before phosphate release[24,25]. The released motor then returns to its pre-powerstroke position so that the cycle can repeat. Images rendered from atomic structures by Graham Johnson (fiVth media: www.FiVth.com).

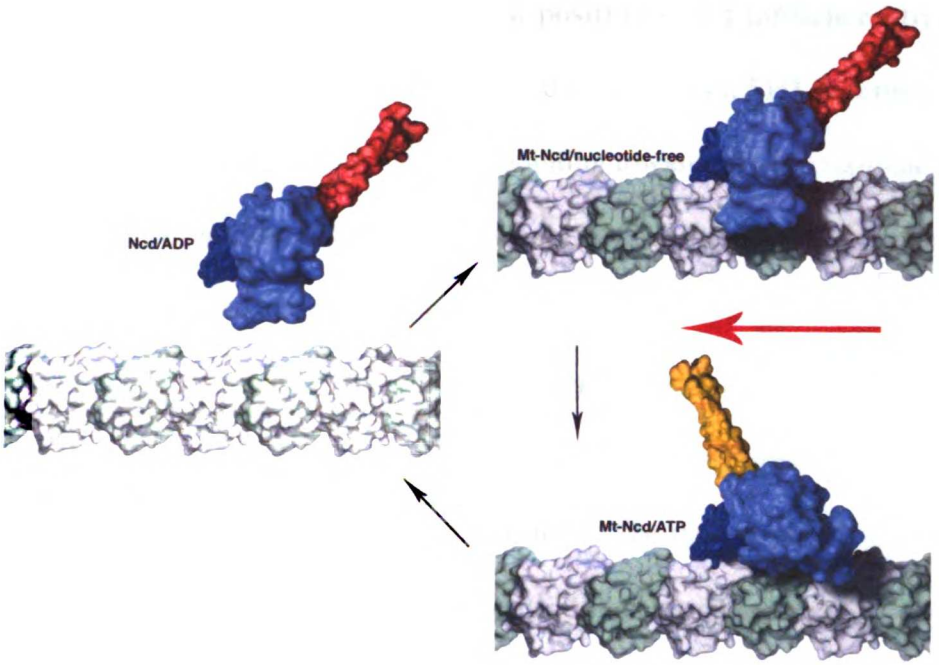

Supplementary Fig. 1: The Ncd neck position is not influenced by adjacent motors. a, Cryo-EM map of the 281-700 a.a. Ncd construct with a SH3 N-terminal tag in the presence of apyrase. An elongate neck density pointing towards the microtubule plus-end is observed. For this construct, the distal part of the neck/SH3 density (labeled N) appears to overlap with the unbound head density of another motor on the adjacent filament (H_A), implying a potential interaction with the SH3 domain which could contribute to the stability of the neck. **b,** Cryo-EM map of the 281-700 a.a. Ncd construct without SH3 tag (N-terminal His_6 tag only) shown in the same orientation as in **(a).** For this construct, the distal part of the neck density (N) does not overlap with the head density of an adjacent motor (H_A). Difference density maps also confirm that the position of the neck relative to the motor domains is identical in (A) and (B) (not shown). This rules out the possibility that an artifactual SH3-head interaction contributed to the position and/or stability of the neck. **c,** Cryo-EM map of the Ncd-SH3 construct in the presence of ADP- AlF_4^-, shows no density overlap between the neck density (N) and adjacent motors (H_A).

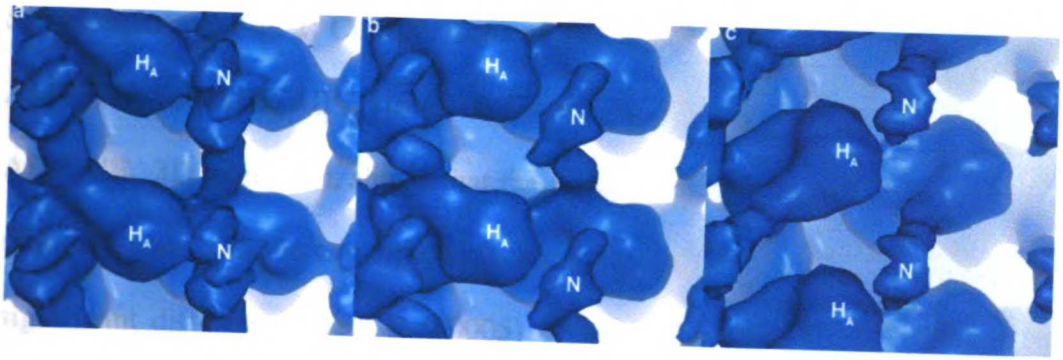
a
H_A
N
H_A
N
b
H_A
N
H_A
N
c
N
H_A
N
H_A

Supplementary Fig. 2: Comparisons of WT maps reveal similar neck conformation for AMPPNP and ADP-AlF_4^- states. a, Overlay of WT 3D map AMPPNP (blue) with the WT ADP-AlF_4^- 3D map (red), shows that the density for the neck and unbound heads are in the same orientation in the two structures. **b,c** Statistical difference maps represent statistically significant differences (red, $P<0.0005$) between 3D maps of Ncd-microtubule complexes compared using a students t test. **(b)** Statistical difference maps comparing WT nucleotide-free and the WT AMPPNP 3D maps (red) superimposed on the WT AMPPNP map (transparent blue). The two peaks labeled H_0 and H_{ATP} are associated with the rotation of the unbound head between the nucleotide-free and AMPPNP states. The two peaks labeled and N_0 and N_{ATP}, reflect the position of the neck in the nucleotide-free and AMPPNP states respectively. **(c)** Statistical difference maps comparing WT nucleotide-free and WT ADP-AlF_4^- 3D maps (red) superimposed on the ADP-AlF_4^- map (transparent blue). Peaks are labeled as in **(b)**. The same difference peaks observed in the comparison between the nucleotide-free and AMPPNP maps **(b)** can be seen here, implying that the head and neck occupy similar positions in both nucleotide states.

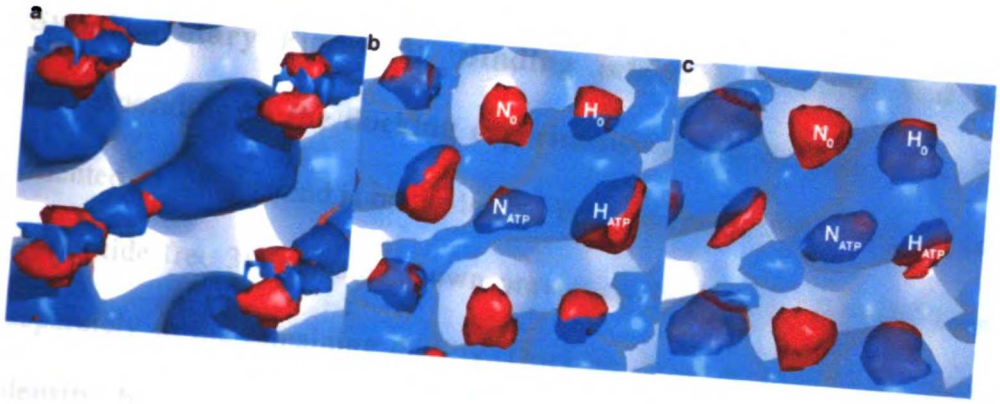

Supplementary Figure 3: Binding interface between Ncd and microtubule corresponding to the docking experiments shown in Figs. 1d-f. The microtubule is oriented so the plus-end is on the left. **a,** Wildtype Ncd-ADP structure[5] (dark blue) docked to nucleotide-free 3D maps as shown previously (Fig. 1d.). Tubulin[6] (orange) was docked separately to the remaining density. Docking shows a good fit for both tubulin and Ncd density. **b,** Close-up view of the region boxed in (A) shows more detailed view of the interface between the bound motor domain and tubulin. Predicted microtubule binding elements are highlighted, L8 (yellow), L11-α4-L12 (light blue) and L2 (red) (*4,5*).

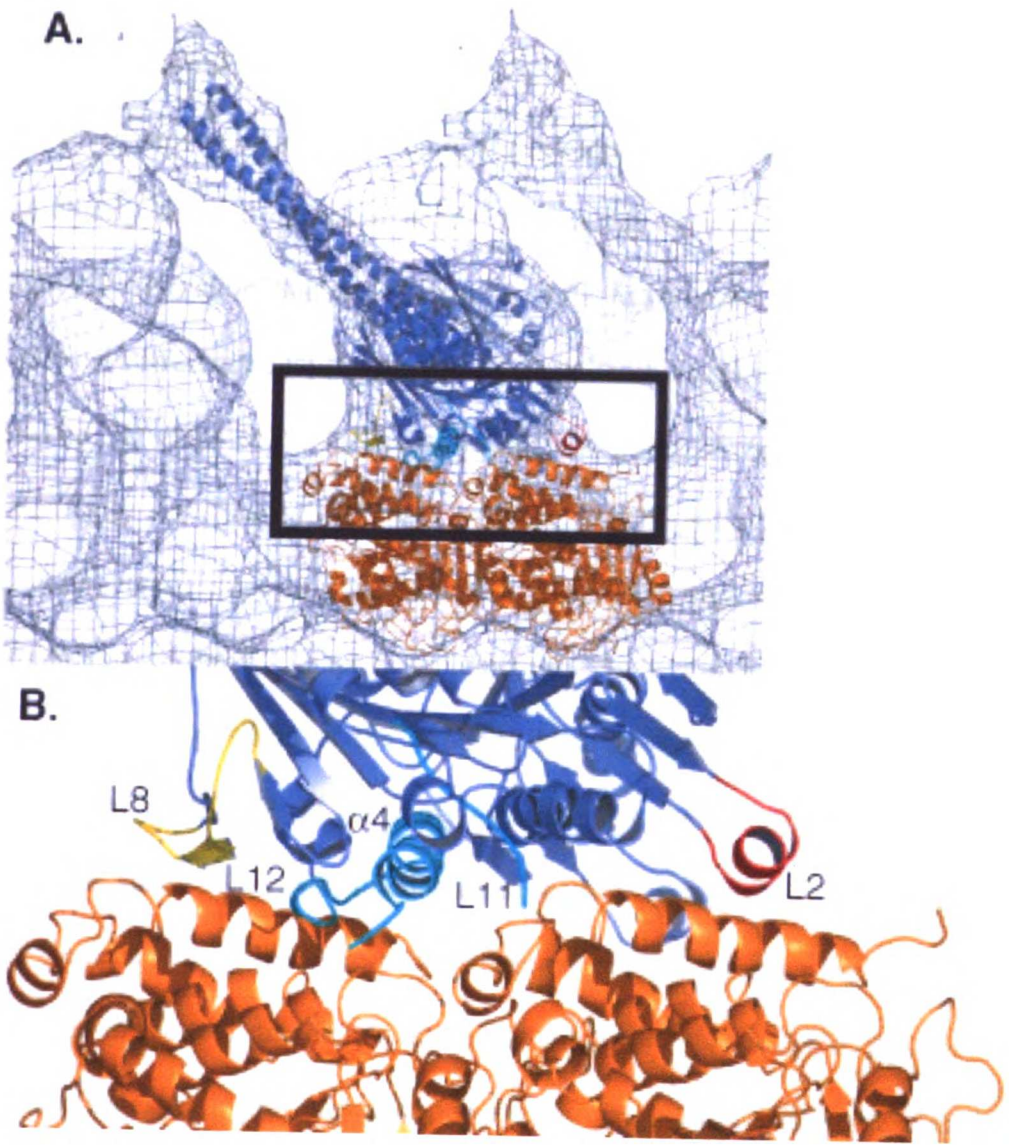

Supplementary Figure 4: Comparisons of Ncd N340K EM maps consistent with model for bidirectional motility (see text). a, 3D maps of N340K in the presence of 5 mM AMPPNP, show a clear definition of the microtubule-bound head, but no neck density and a less clearly defined detached head. **b,** Overlay between N340K ADP-AlF_4^- (blue) and AMPPNP (red) show that the orientation of the heads in the two structures are identical. **c,d** Statistical difference maps representing statistically significant differences (red, $P<0.0005$) between 3D maps of N340K-microtubule complexes compared using a students t test. c, Statistically significant differences between N340K nucleotide-free and N340K AMPPNP 3D maps (red) superimposed on the AMPPNP map (transparent blue). As in the comparisons of the WT maps (Supplementary Fig. 2 b,c), there are two peaks (H_0 and H_{ATP}) attributable the position of the unbound head in the absence of nucleotide (H_0) and the presence of AMPPNP (H_{ATP}) implying some net rotation of the unbound head between nucleotide states. However, in contrast to the WT maps, only a single peak (N_0), associated with the neck density in its pre-powerstroke position, is seen with the NcdN340K mutant. As described in the text, the details in the raw maps of the NcdN340K protein suggest that the neck occupies both pre- and post-powerstroke positions in the nucleotide-free state. The presence of a pre-powerstroke peak (N_0) is consistent with the notion that the pre-powerstroke state is significantly populated in the nucleotide-free state but not significantly populated in the AMPPNP state. The absence of a peak corresponding to a post-powerstroke position (N_{ATP} in Supplementary Fig. S2b,c) indicates that this conformation is equally populated in the nucleotide-free and AMPPNP states. **d,** Statistical difference maps comparing N340K nucleotide-free and N340K ADP-AlF_4^- 3D maps (red) superimposed on the ADP-AlF_4^- map (transparent blue), are nearly identical to the N430K nucleotide-free/

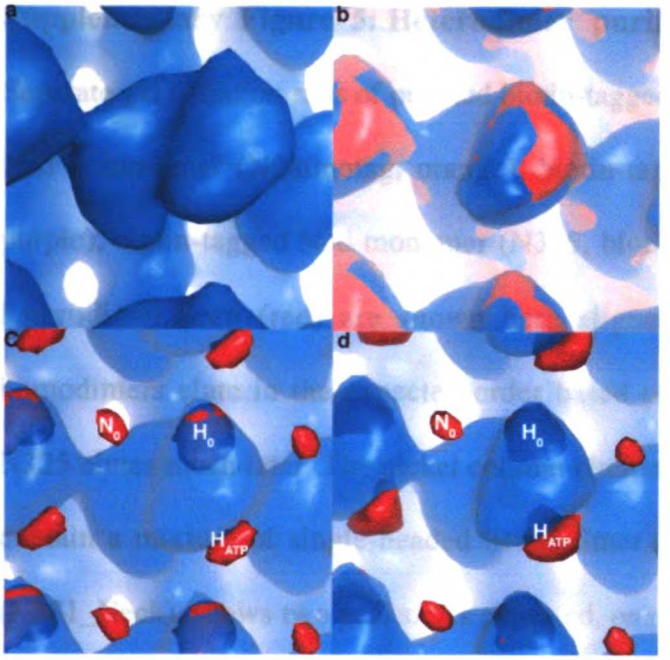
a
b
c
d
N_δ
H_δ
H_{ATP}
N_δ
H_δ
H_{ATP}

Supplementary Figure 5: Heterodimer purification and motility experiments. a, Separate gel filtration runs of purified biotin-tagged Ncd homodimer (N281, black), untagged Ncd homodimer (N280notag, orange), biotin-tagged Ncd neck homodimer (N280_Neck, purple), biotin-tagged Ncd monomer (N325, blue), and the nickel column elution from the heterodimer prep (red) are shown here aligned and scaled (see Methods). Purified homodimers elute in the expected order based on their sizes, whereas the Ncd monomer N325 elutes much later. The nickel column elution from the heterodimer prep, which should contain a mixture of single-headed heterodimer (N280_Het) and tagged neck homodimer (N281_Neck), shows two peaks. As expected, one of the peaks elutes at the same position as N281_Neck. The second peak, indicated with an arrow, is unique to this preparation and elutes in a position intermediate between N281_Neck and N280notag, as would be predicted for N280_Het. Gel electrophoresis of these fractions confirmed that both the motor domain and the tagged neck domain elute in the N280_Het fraction (not shown). The fraction indicated by this peak was used in all N280_Het experiments. **b,** Diagram of typical gliding assay shown (see also methods). Glass surface represented with light blue, grey circles represents combination of Streptavidin and biotinylated BSA bound to the glass, and a rhodamine-labeled microtubule is shown. The gel filtration purified heterodimer (N280_Het) and two possible contaminants (N280notag and N281_Neck) are shown here to demonstrate how they would be predicted to interact with the glass and or microtubule in the gliding assay. The figure demonstrates that only N280_Het would be predicted to support microtubule gliding under these conditions, since it is the only dimer in this mixture that has both a biotin tag to couple it to the glass slide and a motor domain to bind microtubules. Table showing results of gliding assays with the constructs purified constructs shown in (a),

which confirm that only N280_Het, N281, and N325 (the tagged Ncd homodimer and monomer respectively) can support gliding of microtubules as predicted from design of gliding assay. The absence of microtubule binding in the presence of both N280notag and N281_neck suggest that recombination of the polypeptide does not occur and that the aggregation of the two homodimers is not responsible for the motility observed in the single-headed heterodimer containing fractions. Comparison of N280_Het gliding velocity to that of the Ncd dimer (N281) and monomer (N325) show that the single-headed heterodimer behaves more like the dimer, implying that coiled-coil interactions play a larger role then the unbound head in determining the velocity of the motor. The slow movement observed in the monomer (N325) is not likely to be random since experiments with polarity-marked microtubules indicate these motors move towards the minus-end.

A.

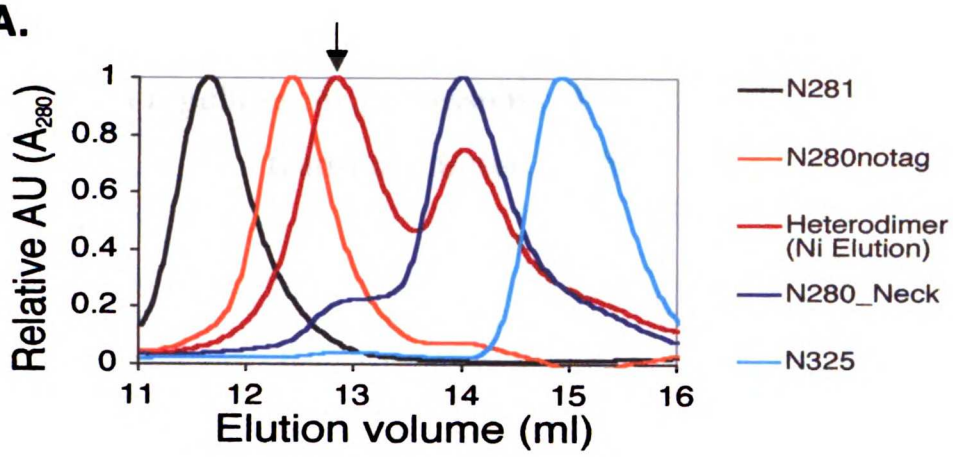

B.

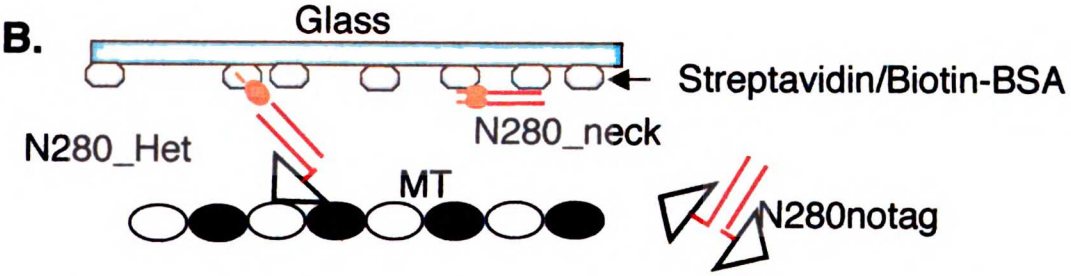

Construct	Gliding Assay
N280notag	No MT Binding
N280_Neck	No MT Binding
N280notag + N280_Neck	No MT Biding
N280_Het	v = 97 ± 18 nm/s
N281 (dimer)	v = 97 ± 18 nm/s
N325 (monomer)	v = 4 ± 3 nm/s

CHAPTER 2

Auto-inhibition regulates the processivity of the *C. elegans* intraflagellar transport motor, OSM-3

The work presented in Chapter 2 is the result of a collaboration between myself, Dr. Miki Imanishi, and Dr. Arne Gennerich. Dr. Imanishi designed the constructs used in the study, and did the ATPase assays and sucrose gradients. I was responsible for the single molecule fluorescence and gliding assay experiments. Dr. Arne Gennerich performed the optical trap experiments. Dr Imanishi and I contributed equally to this projected and have submitted this chapter for publication as co-authors.

SUMMARY

OSM-3 is a Kinesin-2 family member from *Caenorhabditis elegans* that is involved in intraflagellar transport (IFT), a process essential for the construction and maintenance of sensory cilia (Cole et al., 1998; Perkins et al., 1986; Shakir et al., 1993; Snow et al., 2004). OSM-3 moves IFT particles at a velocity of 1.3 μm/s in vivo (Snow et al., 2004); however, the motility of OSM-3 has not been characterized in vitro. Here, using a single molecule fluorescence assay, we show that bacterially-expressed OSM-3 GFP does not move processively (multiple steps along a microtubule without dissociation). However, a single point mutation in a predicted hinge region of the OSM-3 coiled-coil stalk, as well as a deletion of that hinge, activates robust processive movement of OSM-3 at velocities similar to IFT cargo transport in vivo. The processivity of wild-type OSM-3 also can be activated by attaching the motor to beads in an optical trap, a situation that may mimic attachment of OSM-3 to its IFT cargo. Sucrose gradient analysis reveals that OSM-3 adopts a compact conformation that becomes extended in the hinge mutants or at high salt. We propose that the processivity of OSM-3 is repressed by an intramolecular interaction that involves folding about a central hinge and that IFT cargo binding relieves this auto-inhibition in vivo.

INTRODUCTION

Sensory cilia are crucial for chemosensory function in *C. elegans* neurons, and defects in human cilia function can contribute to diseases such as Bardet-Biedl Syndrome (BBS) (Ou et al., 2005a). In these chemosensory neurons, the assembly and maintenance of sensory cilia depends upon intraflagellar transport of particles containing structural and signalling proteins (Snow et al., 2004). Anterograde IFT transport is driven by two Kinesin-2 family members: heterotrimeric kinesin-II (Cole et al., 1993) and homodimeric OSM-3 (Signor et al., 1999). The activities of these two motors must be carefully regulated, since both motors cooperate to move IFT particles along the 'middle segment' of the cilia consisting of double microtubules, while only OSM-3 transports IFT particles along the 'distal segment' consisting of single microtubules (Snow et al., 2004). However the mechanism of such regulation is not yet understood.

RESULTS

Here, we have characterized the motile properties of a recombinant OSM-3 construct consisting of full length OSM-3 (a.a. 1-699) with a C-terminal GFP (Fig. 1). As expected, OSM-3 was an active plus-end-directed motor in a microtubule gliding assay, although the velocity of movement (0.3 μm/s) in this gliding assay was lower than IFT transport by OSM-3 in the distal segment(Snow et al., 2004). The ATP hydrolysis k_{cat} of the full length OSM-3 motor was only 4 ATP/s/head, much slower than would be expected for a motor capable of moving 300-1300 nm/s (assuming that it takes 8 nm steps per ATP hydrolyzed as shown for Kinesin-1(Schnitzer and Block, 1997)). We next examined OSM-3 processivity by imaging single GFP-labelled molecules using a total internal reflection fluorescence (TIRF) microscope. In this assay, a truncated construct of Kinesin-1 (K530; Table 1) fused to GFP exhibited numerous processive movements with an average run length of 1.2 mm, similar to previous results(Romberg et al., 1998; Thorn et al., 2000). In contrast, full length OSM-3 rarely showed any processive runs.

OSM-3's lack of processivity is somewhat surprising, since many dimeric motors involved in long range transport are processive in vitro(Howard et al., 1989; Klopfenstein et al., 2002; Mehta et al., 1999; Tomishige et al., 2002; Zhang and Hancock, 2004). Extensive in vitro studies on the long range, unidirectional processivity of Kinesin-1 and Kinesin-3 have identified three critical determinants of processivity: (i) the presence of a stable "neck coiled-coil" that joins the two kinesin motor domains immediately after the neck linker (kinesin's mechanical element)(Al-Bassam et al., 2003; Romberg et al., 1998), (ii) the ability

of the two motor domains to coordinate their ATPase cycles(Hackney, 1995; Ma and Taylor, 1997), and (iii) the presence of intramolecular interactions that inhibit processivity(Al-Bassam et al., 2003; Coy et al., 1999; Friedman and Vale, 1999; Hackney et al., 1992). We sought to test whether any of these possible mechanisms could explain the lack of processivity by OSM-3.

We initially suspected that an unstable neck may underlie the lack of OSM-3 processivity, since the neck coiled-coil of OSM-3 is over 2 heptads shorter and predicted to be much weaker than the neck coiled-coil of Kinesin-1 (Fig. 1b). The putative OSM-3 neck coiled-coil also is less positively charged than the neck coiled-coil of Kinesin-1, a factor shown to enhance its processivity(Thorn et al., 2000). We tested the hypothesis that a weak coiled-coil may be responsible for the lack of processivity of OSM-3 by fusing the putative neck coiled-coil of OSM-3 (and the subsequent C-terminal stalk and tail domains) to the motor domain and neck linker of Kinesin-1 (K-O, see Table 1). We reasoned that if the OSM-3 neck was incompatible with processivity, then K-O should be a non-processive motor. Contrary to this prediction, K-O molecules moved processively in the single molecule TIRF assay, with similar velocities (0.5 ± 0.2 μm/s), albeit with reduced run lengths (0.4 μm), compared to K530 (0.7 ± 0.3 μm/s, 1.2 μm). The processivity of K-O suggests that the OSM-3 neck coiled-coil is not responsible for the lack of processivity in OSM-3.

We next tested if the OSM-3 motor domain was incompatible with efficient processive motility by fusing the OSM-3 motor domain (catalytic core and neck linker) to the

neck coiled-coil and stalk of Kinesin-1 (O-K, see Table 1). O-K exhibited robust processive movement with an average run length (2.6 μm) that was ~2-fold higher than that of K530. The velocity measured in the single molecule fluorescent assay (1.5 ± 0.3 μm/s) was similar to the velocity of OSM-3 cargo in vivo (1.3 ± 0.2 μm/s), suggesting that O-K may be mimicking the in vivo function of the motor. Thus, the OSM-3 motor domain is compatible with processivity in a dimeric construct that lacks its native stalk/tail domain. Interestingly, the O-K ATPase rate (k_{cat}, 75 ATP/s/head) was an order of magnitude greater than that of wild type OSM-3 (k_{cat}, 4 ATP/s/head). This difference in rates indicates that some element C-terminal to the motor domain of OSM-3 is inhibiting its catalytic activity, and likely the processivity of the motor as well.

To test if the tail domain might inhibit the processivity of OSM-3, we made a construct of OSM-3 lacking the tail domain (OSM-3 aa.1-555) but found that it was an unstable dimer under conditions of the TIRF assay (low nanomolar range; data not shown). An alternative strategy for investigating a possible auto-inhibition of OSM-3 processivity was suggested by a comparison with Kinesin-1. The processivity of Kinesin-1 is inhibited by an auto-inhibitory interaction between its neck coiled-coil and tail domains(Coy et al., 1999; Friedman and Vale, 1999; Hackney, 1995). The interaction of these distant N- and C-terminal elements is achieved by folding about a flexible hinge in the stalk (H2 in Figure 1b). Deletion of this hinge prevents auto-inhibition and restores processivity to the motor(Friedman and Vale, 1999). A comparison of the overall architecture of the Kinesin-1 and OSM-3 stalk suggests the presence of an analogous hinge in OSM-3 (H2 in Fig. 1b). Therefore, we wondered if deletion of H2 and the in phase fusion of the adjacent coiled-coils

(CC1 and CC2, Fig. 1b) could restore processivity to OSM-3. Strikingly, this construct (OSM-3-ΔH2) exhibited robust processive movement with long run lengths (~2 μm; Table 1) in the single molecule TIRF assay and displayed similar elevated ATPase rates (~70 ATP/s/head) to O-K. The dramatic activation of processivity in OSM-3-ΔH2 demonstrates that the OSM-3 motor, in the absence of any fusion to Kinesin-1, has an intrinsic potential for processive motion. These results also show that H2 plays a critical role in repressing the processivity of OSM-3.

Having demonstrated the importance of H2 for the regulation processivity in vitro, we searched through OSM-3 alleles for mutations in H2 that produce chemosensory defects in *C. elegans(Snow et al., 2004)*. We noticed one allele (*sa125*) in H2 that changed a glycine to a glutamatic acid (G444E). When this H2 point mutation was introduced into full length OSM-3 (OSM-3-G444E), we found a striking activation of processivity and ATPase activity, similar to that observed with the deletion of the entire H2 region. The velocity of OSM-3-G444E (1.1 ± 0.2 μm/s) is also similar to that of OSM-3 driven IFT transport in vivo, implying that this mutation could activate OSM-3 in a manner similar to its activation in vivo. The dramatic activation of processivity by a single point mutant implies that a specific conformation of H2 is required for regulation of OSM-3 processivity.

In Kinesin-1, H2 facilitates a conformational transition between a compact, non-processive form (S=6.7) and a more extended, processive form (S=5.1)(Hackney et al., 1992). The compact to extended conformational transition is favored by cargo binding(Coy et al., 1999) and high ionic strength(Hackney et al., 1992). To investigate if a similar

conformational change could underlie the regulation of OSM-3 processivity, we examined the hydrodynamic properties of wild type and mutant OSM-3 by sucrose gradient sedimentation. Similar to Kinesin-1, OSM-3 sediments with a higher $S_{20,w}$ value at low ionic strength ($S_{20,w}$ = 7.9 at 0 M NaCl) than at high ionic strength ($S_{20,w}$ = 6.7 at 1 M NaCl), suggesting that it too has compact and extended conformations. In contrast to wild type OSM-3, the H2 mutants (OSM-3-ΔH2 and OSM-3-G444E) sedimented with a low $S_{20,w}$ value ($S_{20,w}$ = 6.5 - 6.9) at both low and high ionic strength. These results suggest that the processive H2 mutants stabilize an extended conformation of OSM-3. We attempted to visualize the two OSM-3 conformations by rotary shadow EM, but unfortunately could not obtain satisfactory images due to aggregation of the motor on the mica surface (J. Heuser, unpublished results). The correlation between the extended conformation of OSM-3 and in vitro processivity suggests that a reversible, auto-inhibitory interaction regulates the motility of OSM-3.

Relief of OSM-3 auto-inhibition in vivo might be stimulated by cargo binding. In order to mimic cargo binding in vitro, we attached wild type OSM-3 and OSM-3-G444E via their C-terminal GFP to beads coated with GFP antibody. Motor-coated beads were then captured by an optical trap and positioned near axonemes immobilized onto a coverslip. As expected, OSM-3-G444E-coated beads moved processively at three different constant loads generated by force feedback (1 - 6 pN; Fig 3a). The continued movement at 6 pN suggests that the motor can exert forces in excess of that value, as thus has similar force producing capability to Kinesin-1(Svoboda and Block, 1994). Wild type OSM-3-coated beads also moved processively, with velocities comparable to OSM-3-G444E at all three force levels

(Figure 3b), implying a similar mechanism. To determine if the bead motion was driven by single or multiple motors, the fraction of moving beads was measured as a function of motor-bead ratio. Poisson statistical analysis clearly revealed that a single OSM-3-G444E or wild type OSM-3 motor is sufficient to move a bead(Svoboda and Block, 1994) (Fig. 3c,d), although wild type OSM-3 required a 60-fold higher motor-bead ratio to yield an equivalent probability of bead movement as OSM-3-G444E. The requirement for a higher concentration of wild type OSM-3 could be due to a lower probability of motor-bead attachment as a result of the folded conformation of the inactivated OSM-3 or due to inefficient activation of the repressed OSM-3 motors by their attachment to the GFP antibody-coated beads. The fact that wild type OSM-3 bound to anti-GFP antibody coated glass slides can move microtubules in a gliding assay also is consistent with the idea that surface attachment can activate repressed OSM-3, although the number of active motors was not investigated in this assay. In summary, our results demonstrate that wild type OSM-3, once relieved of its inhibition by surface attachment, is capable of processive movement.

In conclusion, we have shown that the processive movement and microtubule-stimulated ATP activity of OSM-3 are repressed in solution. ATPase activity and processivity are both dramatically stimulated by mutations in hinge 2, which also change the conformation of the motor from a compact to an extended form. Wild type OSM-3 also becomes processive when attached via its tail domain to beads. Collectively, these results suggest a model in which OSM-3 exists in the cytoplasm in a compact, auto-inhibited state and that binding to an IFT particle relieves this auto-inhibition, converting the motor to an extended conformation and enabling long distance processive movement (Fig. 4). Although

more work will be needed to understand the structural basis of this auto-inhibition, the processivity of OSM-3-Kinesin-1 chimeras (O-K and K-0) suggests that inhibition requires both the OSM-3 motor and stalk/tail domains and perhaps involves interactions between the two. This proposed regulatory mechanism for OSM-3 is similar to that described to Kinesin-1 (Adio et al., 2006). However, these two motors belong to different kinesin classes that share no sequence similarity in their non-motor domains and diverged very early in eukaryotic evolution (Vale, 2003). Kinesin-3 processivity also is repressed by the formation of an intramolecular coiled-coil in its neck region which inhibits dimerization (Al-Bassam et al., 2003). Although the effects on motor activity are not known, heterotrimeric kinesin-II also undergoes a salt dependent conformational shift between a compact and an extended form (Wedaman et al., 1996). Thus, auto-inhibitory mechanisms, although differing in their precise intramolecular interactions, may be commonly employed in motor regulation.

The regulation of OSM-3 processivity is likely to be important for its biological function in vivo. Strongly supporting this connection, the OSM-3-G444E allele (*sa125*), which interferes with auto-inhibition in vitro, behaves indistinguishably from OSM-3 null allele (*sa131*) in *C. elegans* chemosensory neurons (Snow et al., 2004). Further supporting a loss of OSM-3 function, the distal ciliary segment (which is supplied exclusively by OSM-3 transport (Snow et al., 2004)) does not form in OSM-3-G444E mutant animals and IFT particles move along the remaining ciliary segment at velocities similar to IFT particles being transported by heterotrimeric kinesin-II alone (Ou, G. and Scholey, J., unpublished results). While the OSM-3-G444E allele (sa125) behaves as a null in vivo, our in vitro optical trapping experiments show that its velocity and force production are indistinguishable from

the wild type motor. Thus, the most plausible explanation for the in vivo mutant phenotype is a loss of motor regulation, rather than motor domain dysfunction. Two possible mechanisms could explain how a loss of auto-inhibition gives rise to a null phenotype. First, a constitutively active OSM-3-G444E motor may not be able to dock onto IFT cargo. Second, processive OSM-3-G444E motors may constitutively move along microtubules in the neuronal cell body and fail to be delivered to the cilium. Another open question is how OSM-3 is relieved of its auto-inhibition. It has been shown previously that the DYF-1 protein is required to load OSM-3 onto IFT particles (Ou et al., 2005b), but purified DYF-1 did not activate wild type OSM-3 in our single molecule assay (preliminary data, not shown). Thus, the regulatory machinery may require additional proteins or post translation modifications. Consistent with this idea, two novel mutants with a similar phenotype to *dyf-1* and *osm-3* worms were recently identified (G. Ou and J. Scholey unpublished). The ability to study OSM-3 auto-inhibition in vitro and in vivo function in living *C. elegans* provides powerful tools for dissecting the regulatory mechanism of this IFT motor.

METHODS

Cloning and protein preparations.

OSM-3 cDNA was obtained from J. Scholey (U.C. Davis). From this clone, we constructed OSM-3-GFP in a pET-17b plasmid, which encodes amino acid 1-699 of *C. elegans* OSM-3 with a COOH-terminal GFP (S65T variant) followed by a His_6 tag. K530-GFP (aa. 1-530 of Kinesin-1) was derived from K560-GFP[19]. In the O-K construct, a.a. 1-337 of the OSM-3 motor domain were followed by a.a. 337-530 of the K530 stalk. In the K-O construct, a.a. 1-336 of the human Kinesin-1 motor domain were followed by a.a. 338-699 of the OSM-3 stalk/tail. The OSM-3-G444E construct was created by QuickChange mutagenesis. For OSM-3-ΔH2, a.a. 428-447 were removed to maintain a continuous heptad repeat between CC1 and CC2 (Fig. 1). Protein expression and purification were carried out as described(Case et al., 1997). For ATPase assays, single molecule fluorescence and optical trap experiments, and gliding assays, motor proteins were further purified by microtubule affinity (Case et al., 1997). Motor concentration was either determined by Bradford assay or SDS-PAGE using BSA as a standard.

ATPase assays and single molecule fluorescence measurements.

Microtubule-stimulated ATPase activities were measured as described previously (Woehlke et al., 1997) using 1-20 nM of motor and 0-10 μM of microtubules in BRB12 (12 mM Pipes, pH 6.8, 2 mM $MgCl_2$, 1 mM EGTA, 1 mM DTT, 1mM ATP). Hydrolysis of ATP was plotted against microtubule concentration and data were fitted to a Michealis-Menton equation to determine the k_{cat} and K_m MT. The movements of single GFP-fused

kinesin molecules along axonemes were visualized by total internal reflection fluorescence microscopy using BRB25 buffer (BRB12 with 25 mM Pipes) as described previously[Pierce et al., 1999]. The laser power for total internal reflection illumination was 9 mW. Motility was analyzed and corrected for photobleaching using Image-J as described(Thorn et al., 2000). Microtubule gliding assays were performed using glass slide coated with GFP antibodies, and gliding velocities of cy3-labelled microtubules were determined as described(Case et al., 1997).

Hydrodynamic analysis.

Sucrose density centrifugation was performed in BRB25 and 10 μM ATP with 0 or 1 M NaCl . OSM-3 and standard calibration proteins (ovalbumin, 3.7 S; albumin, 4.2 S; and catalase, 11.3 S) were mixed and loaded onto 12-33% sucrose gradients. After centrifugation at 50,000 g for 6 hr using a SW55Ti rotor (Beckman Coulter), fractions were analyzed by SDS-PAGE. $S_{20,w}$ values of the standards were plotted versus their peak sedimentation fraction number and fit to a linear curve. $S_{20,w}$ of OSM-3 motor were calculated based upon their peak sedimentation fraction and the slope of the standard curve.

Optical Trapping assay.

Optical trapping bead assay was carried out using a feedback-controlled single beam trapping microscope. GFP-tagged OSM-3 and OSM-3-G444E were coupled to carboxylated latex beads (0.92 μm diameter, Molecular Probes) via affinity-purified anti-GFP antibodies(Tomishige et al., 2002). Trapped beads were positioned near rhodamine-labeled sea urchin sperm flagellar axonemes immobilized onto a coverslip. Bead displacement was

sampled at 2 kHz with a quadrant photodiode detector. Trap stiffness was calibrated for each trapped bead from the amplitude of the thermal diffusion. Prior to each experiment, the trapped bead was scanned along the x-axis (coinciding with the long axis of the axoneme) across the detection region to obtain the detector's response. Experiments were carried out at dilutions at which the fraction of beads moving was 0.3 or less to ensure measurements on a single molecule level (Svoboda and Block, 1994). Velocities were obtained from the slopes of the displacement traces of the beads moving under constant load. The bead-trap separation during force-clamp measurements was between 50-150 nm depending on applied load (1-6 pN) and trap stiffness (0.022-0.6 pN/nm). The assay solution was 80 mM PIPES (pH 6.8), 2 mM $MgCl_2$, 1mM EGTA, 1 mM Mg-ATP, 1 mg/ml casein, 10 mM DTT, and an oxygen scavenger system (Yildiz et al., 2004).

Constructs	Single Molecule		Gliding	ATPase activity	
	Velocity (μm/s)	Run length (μm)	Velocity (μm/s)	K_{cat} (ATPs/s/head)	K_m MT (μM)
Osm-3	N.D.	N.D.	0.32 ± 0.06	4 ± 1	0.23 ± 0.02
K530	0.7 ± 0.3	1.2	N.D.	29 ± 6	0.29 ± 0.08
K-O	0.5 ± 0.2	0.4	0.30 ± 0.07	33 ± 5	0.20 ± 0.10
O-K	1.5 ± 0.3	2.6	0.48 ± 0.08	75 ± 9	0.13 ± 0.09
OSM_3-ΔH2	0.8 ± 0.2	1.9	0.80 ± 0.10	69 ± 5	0.21 ± 0.06
OSM-3-G444E	1.1 ± 0.2	1.4	0.91 ± 0.09	75 ± 2	0.30 ± 0.10

N.D. Not Determined

Figure 1: Domain architecture of OSM-3 and Kinesin-1 and OSM-3 constructs used in this study **(A)** Domain architecture reveals the positions of the motor and tail domains as well as predicted coiled-coils and hinges (see panel B). Domain sizes are shown roughly proportional to the length of sequence in each domain. Kinesin-1 and OSM-3 sequences are colored red and black, respectively. **(B)** Coiled-coil prediction (based upon COILS(Lupas et al., 1991)) for Kinesin-1 (residues 337-950) and OSM-3 (residue 338-699). Neck, hinge and coiled-coil subdomains are labeled.

Figure 1

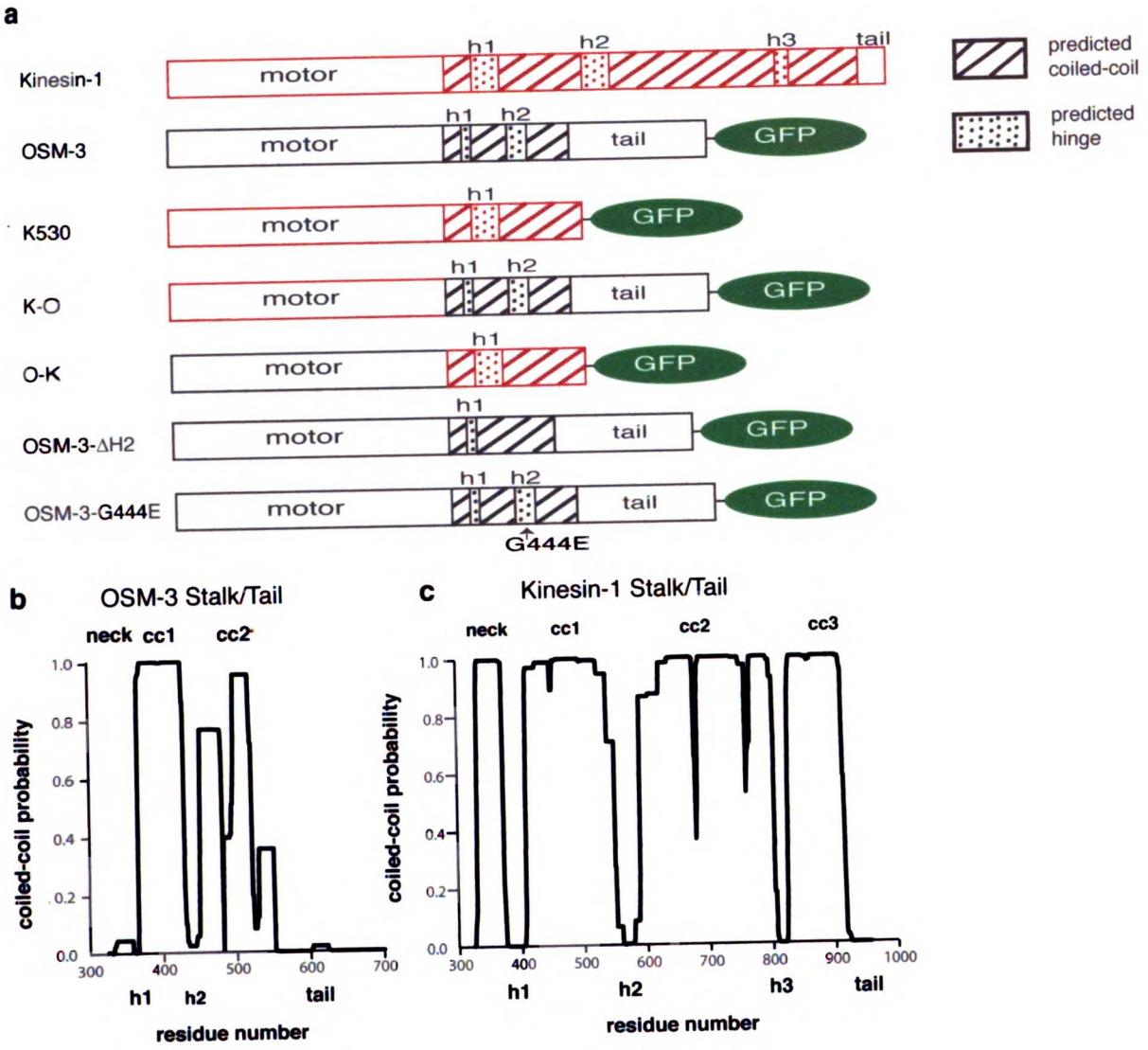
a
Kinesin-1
motor
h1
h2
h3
tail
OSM-3
GFP
K530
K-O
O-K
OSM-3-ΔH2
OSM-3-G444E
G444E
predicted coiled-coil
predicted hinge
b
OSM-3 Stalk/Tail
neck
cc1
cc2
coiled-coil probability
residue number
c
Kinesin-1 Stalk/Tail
cc3

Figure 2: Hydrodynamic properties of wild-type OSM-3 wild type and H2 mutants measured by sucrose gradient sedimentation (**A**) Fractions from sucrose gradients (0 M NaCl) analyzed by SDS-PAGE. Note the shift in the sedimentation peak of OSM-3-G444E compared to wild type OSM-3. Albumin, catalase and ovalbumin were added as hydrodynamic standards. (**B**) Normalized SDS-PAGE band intensity are plotted versus fraction number for OSM-3, OSM-3-ΔH2, and OSM-3-G444E at O M NaCl and wild type OSM-3 at 1 M NaCl. (**C**) Table summarizing the $S_{20,w}$ values measured for the three constructs at O and 1 M NaCl. Values represent mean ± s.d. for 3-4 independent experiments.

a

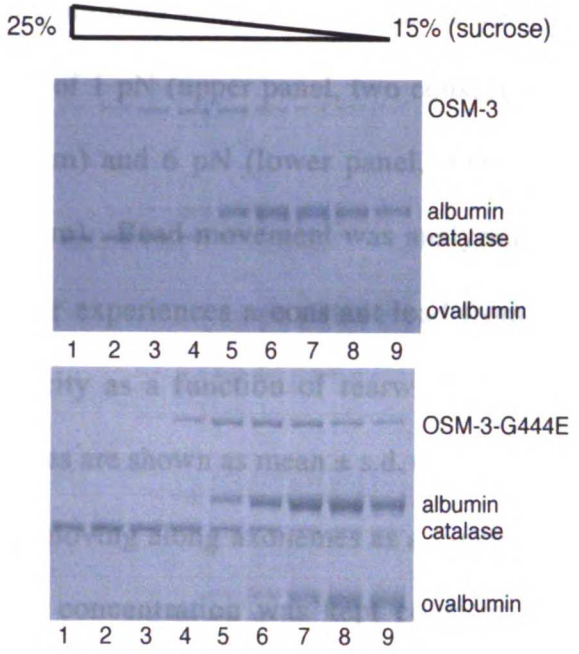

b

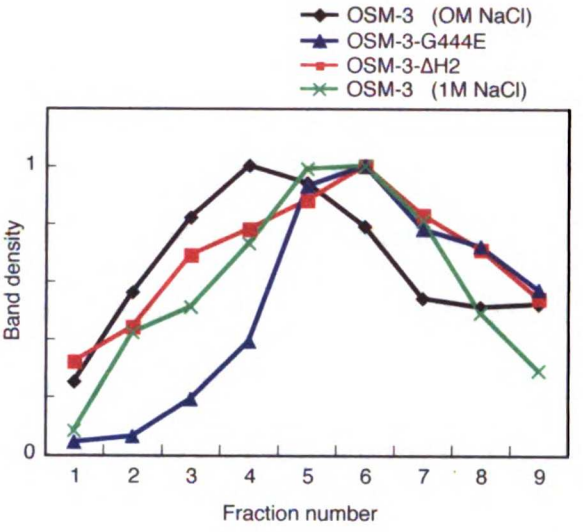

c

Constructs	Sucrose Gradient $S_{20,w}$	
	[NaCl]	
	0 M	1 M
OSM-3	7.9 ± 0.4	6.7 ± 0.2
OSM-3-G444E	6.9 ± 0.3	6.5
OSM-3-ΔH2	6.7 ± 0.3	6.5

Figure 3: Single wild-type Osm3 and Osm3-G444E are processive motors in an optical trapping bead assay. **(A)** Processive movement of wild-type Osm3 under constant rearward load of 1 pN (upper panel, two consecutive runs from the same record are shown; k=0.024 pN/nm) and 6 pN (lower panel, three runs from the same record are depicted; k=0.044 pN/nm). Bead movement was analyzed in a detection area of ± 200 nm within which the motor experiences a constant load from the feedback-controlled optical trap. **(B)** Motor velocity as a function of rearward load for both wild-type OSM-3 and OSM-3-G444E. Values are shown as mean ± s.d. **(C)** The fraction of wild-type Osm3-coated beads binding to and moving along axonemes as a function of the ratio of motor-to-bead concentration. The bead concentration was kept constant for all measurements at 4 pM, while the motor concentration was varied. The solid line depicts the fit to the Poisson distribution $1-\exp(-\lambda C)$ for one or more motor molecules (Svoboda and Block, 1994) (reduced $\chi^2 = 0.31$). Dashed line: fit to the distribution $1-\exp(-\lambda C)-(\lambda C)\exp(-\lambda C)$ for two or more molecules (reduced $\chi^2 = 2.93$). Data values are displaced as the mean $\pm \sqrt{[f(1-f)/N]}$, with N being the number of beads tested. **(d)** Fraction of beads moving as a function of the ratio of Osm3G444E and bead concentration. The solid line depicts the fit to the Poisson distribution for one or more motor molecules (reduced $\chi^2 = 0.08$) and the dashed line the fit to the distribution for two or more motor molecules (reduced $\chi^2 = 2.01$), respectively.

Figure 3

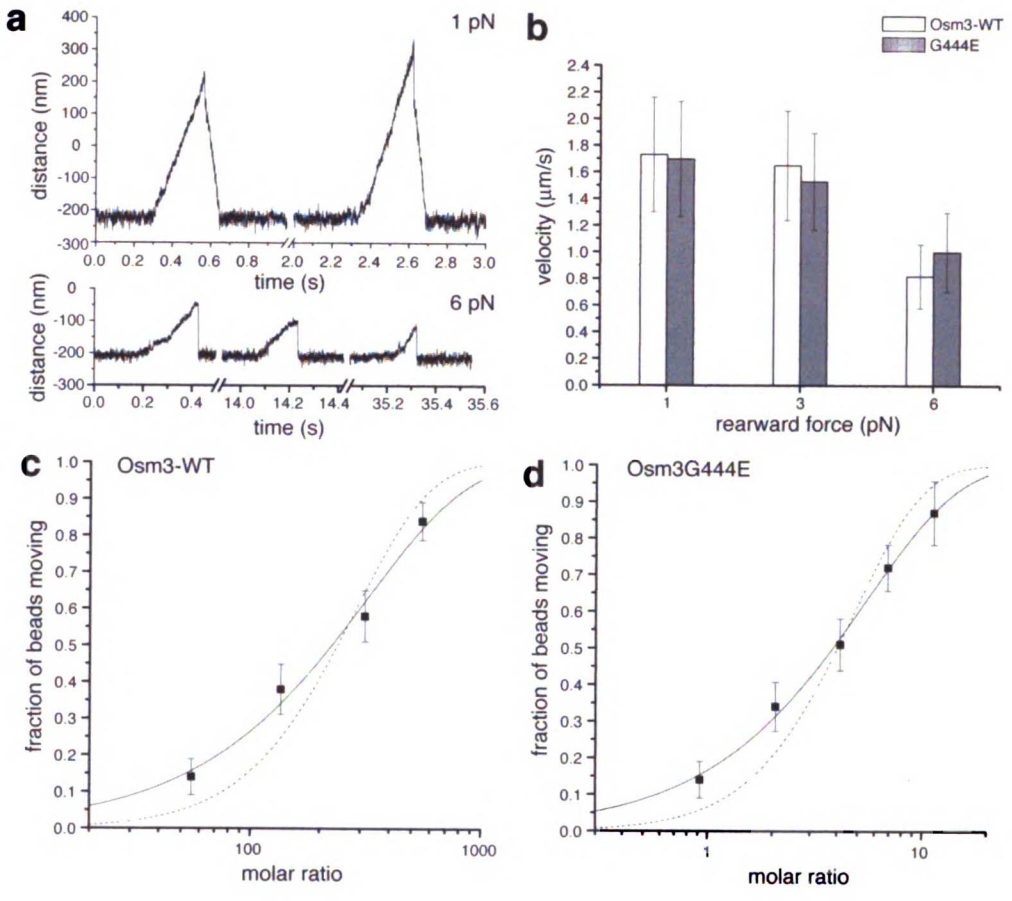
a
1 pN
distance (nm)
time (s)
6 pN
b
Osm3-WT
G444E
velocity (µm/s)
rearward force (pN)
c
Osm3-WT
fraction of beads moving
molar ratio
d
Osm3G444E
fraction of beads moving
molar ratio

Figure 4: Auto-inhibitory model of OSM-3 motor regulation. Cargo-attachment converts the intramolecular folded, repressed OSM-3 into the extended conformation that can undergo processive motion. See text for details.

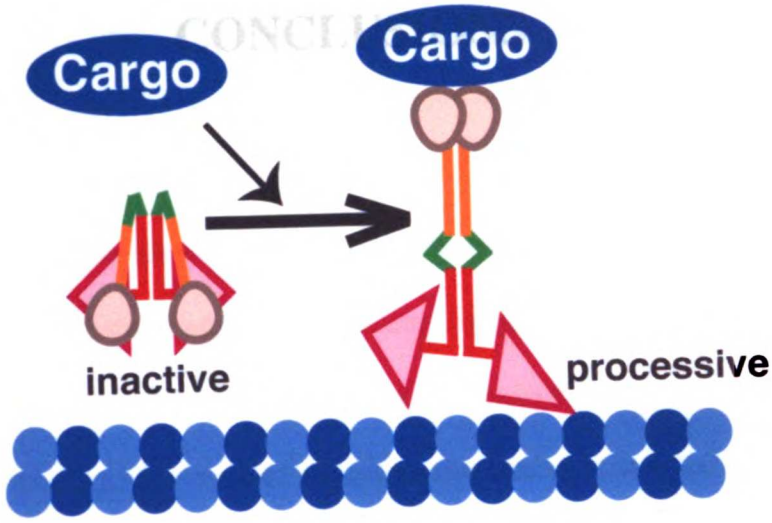
Cargo
Cargo
inactive
processive

Implications of our study of Ncd

We initially set out to determine how Ncd could utilize a highly conserved motor domain to move in opposite direction of Kinesin-1 and the other plus-end directed kinesins. Our work shows that although the conformational change required for Ncd motility is coupled to the same step of the ATPase cycle (ATP binding) as the conformational change required for Kinesin-1 motility, the nature of the conformational change is quite different. While Kinesin-1 motility is driven by a conformational change in its neck linker from an undocked to a docked conformation (Rice et al., 1999), the motility of Ncd is driven by a rotation of its neck coiled-coil which acts as a lever arm, a force production mechanism that is similar to that of the myosin II motor along actin filaments (Suzuki et al., 1998; Uyeda et al., 1996). Remarkably, the nature of the Ncd lever arm (a coiled-coil) differs significantly from that of Myosin II (a helical motif stabilized by binding of light chains) suggesting that Ncd and Myosin II convergently evolved a similar strategy for motility. The directionality of Myosin II can also be reversed by the evolution of a modified mechanical element as is the case for the myosin VI motor which move in the opposite direction as Myosin II (Menetrey et al., 2005). Thus the evolution of a unique mechanical element that can take advantage of existing conformational changes in the catalytic core may be a common mechanism by which motors can develop new directionality.

Both Ncd and Myosin II are non-processive motors (deCastro et al., 2000; Pechatnikova and Taylor, 1999). While Ncd is designed for microtubule cross-bridging and tension development in microtubule based meiotic or mitotic spindles (Sharp et al., 1999b),

Myosin II is designed for cross-bridging and tension between myosin and actin filaments. Interestingly the kinesin-5 family of motor proteins which is also involved in cross-bridging of microtubules (Sharp et al., 1999a) has been shown to have a significantly lower processivity then Kinesin-1 (Crevel et al., 1997; Valentine et al., 2006), although the directionality of this motor is likely to be determined by neck linker docking as in Kinesin-1 (Rosenfeld et al., 2005). In contrast to these cross-bridging motors, motors involved in long range transport tend to be highly processive. These processive motors include: Kinesin-1 (Howard et al., 1989), Kinesin-2 (Zhang and Hancock, 2004), Kinesin-3 (Klopfenstein et al., 2002), Myosin-V (Mehta et al., 1999), Myosin-VII (Yang et al., 2006), and Cytoplasmic Dynein (Mallik et al., 2004). Intriguingly Myo-VI acts as both a transporter and a cross-bridger, and may have both a processive mechanism for cargo transport under low loads and a non-processive mechanism for tension generation under high loads (Altman et al., 2004). Thus a common theme emerges from these mechanistic studies of motor proteins that the processivity of a motor is intricately related to it primary function as either a processive transporter, which requires a small number of motors operating over a long distances and low loads, or as a non-processive tension generator which requires a large number of motors operating over a short distance under high loads.

Implications of our OSM-3 study

Our study of OSM-3 suggest that an intramolecular interaction facilitated by a folding about a critical hinge region inhibits OSM-3 processivity. OSM-3 is one of several motors to have a mechanism for regulating its processivity. This mechanism of processivity

regulation of Kinesin-1 (Friedman and Vale, 1999; Hackney et al., 1992) is similar to what we discovered for OSM-3, although there coiled-coils share little similarity in either sequence or design. Kinesin-3 processivity is stimulated by dimerization (Tomishige et al., 2002) and can be repressed by the formation of an intramolecular coiled-coil in its neck region (Al-Bassam et al., 2003). The processivity of Myo VI may also be stimulated by dimerization (Park et al., 2006). The processivity of Dynein is significantly enhanced by the binding of its dynactin complex cargo (King and Schroer, 2000). For all these motors, cargo binding has been suggested as a mechanism for relieving processivity inhibition. Thus, processivity regulation appears to be a recurring theme in motor regulation and could serve as a partial explanation for some of the diversity of the motor families. The regulation of processivity by cargo binding makes sense from an energetic perspective, since motors not attached to cargo should not be wasting ATP or taking up precious space on the microtubule. Perhaps the diversity of processivity regulation mechanisms is reflective of the diversity of cargo transported by Kinesins, which clearly need to be transported only in specific contexts. These processivity regulation mechanisms have been proposed primarily based on in vitro studies, so more in vivo studies will be needed in order to determine if and if so how cargo binding releases motors from there inhibited states.

The observation that the OSM-3-G444E allele (*sa125*) which is constitutively processive in vitro, behaves behaves indistinguishably from OSM-3 null allele (*sa131*) in *C. elegans* chemosensory neurons (Snow et al., 2004) (Gaugshou and J. Scholey unpublished), provides tantalizing, though indirect, evidence for the importance of processivity regulation in vivo. I believe that the ability to combine insights from single molecule biophysics

experiments in vitro, with the genetics and microscopy of IFT transport and cilia formation in living *C. elegans* worms provides a unique opportunity to determine how OSM-3 in specific, and processivity in general is regulated in vivo. One approach would be to attempt to reconstitute the activation of OSM-3 processivity in vitro using potential cargo binding proteins identified in screens for phenotypes similar to the OSM-3 null allele. As discussed in chapter 2, several of these alleles now exist, and though the protein we tested, DYF-1 (Ou et al., 2005a), did not stimulate the processivity of OSM-3, it is possible that these new alleles or a combination of these with DYF-1 could be sufficient for activating OSM-3 processivity in vitro.

Reflection on the purpose of motor diversity

Of the 12 Kinesin motor families involved in motility and force production along microtubules, the mechanism for five of them have been characterized to some degree in vivo, Kinesin-1 (Rice et al., 1999), Kinesin-3 (Klopfenstein et al., 2002; Tomishige et al., 2002), Kinesin-5 (Valentine et al., 2006), Kinesin-14 (Ncd, chapter 1), Kinesin-2 (Osm-3, chapter 2). All these studies reveal differences in either intrinsic processivity, or how processivity is regulated. In the case of Ncd and Eg5, the processivity of the motors is intrinsically low in order to generate motors which are adapted for tension generation. In the case of Kinesin-1, Kinesin-2, and Kinesin-3 the motors are intrinsically processive but all have a unique mechanism to ensure that processivity can be turned on in the appropriate context, presumably when the motor is bound to cargo. A similar pattern of processivity differentiation has been observed among members of the myosin super family of motor

proteins. Thus, processivity seems to be a critical factor in the diversity of motor function and regulation.

For all five of these well-studied motor families the sequence differences that are critical for processivity are located either in or immediately adjacent to the coiled-coil domain. Thus, a careful comparison of the coiled-coil domain of Kinesin within and among families may be the best strategy for predicting kinesins with novel functions or regulation mechanisms. This analysis could include searching for conserved topological features such as hinge regions, protein-protein interaction motifs, phosphorylation sites or potential intramolecular interactions sites. One tantalizing idea would be to search for a processive minus-end-directed kinesins. Plants lack Dynein, yet seem to have many different minus-end-directed kinesins, and one organism (Arabidopsis) has 21 Kinesin-14's (Reddy and Day, 2001). It is tempting to think that a Kinesin-14 varient could take over Dynein's role as the processive minus-end directed transport in Arabidopsis or other plant species.

REFERENCES

Adio, S., Reth, J., Bathe, F., and Woehlke, G. (2006). Review: regulation mechanisms of Kinesin-1. J Muscle Res Cell Motil *27*, 153-160.

Al-Bassam, J., Cui, Y., Klopfenstein, D., Carragher, B. O., Vale, R. D., and Milligan, R. A. (2003). Distinct conformations of the kinesin Unc104 neck regulate a monomer to dimer motor transition. J Cell Biol *163*, 743-753.

Altman, D., Sweeney, H. L., and Spudich, J. A. (2004). The mechanism of myosin VI translocation and its load-induced anchoring. Cell *116*, 737-749.

Arnal, I., Metoz, F., DeBonis, S., and Wade, R. H. (1996). Three-dimensional structure of functional motor proteins on microtubules. Curr Biol *6*, 1265-1270.

Asbury, C. L., Fehr, A. N., and Block, S. M. (2003). Kinesin moves by an asymmetric hand-over-hand mechanism. Science *302*, 2130-2134.

Barrett, J. G., Manning, B. D., and Snyder, M. (2000). The Kar3p kinesin-related protein forms a novel heterodimeric structure with its associated protein Cik1p. Mol Biol Cell *11*, 2373-2385.

Case, R. B., Pierce, D. W., Hom-Booher, N., Hart, C. L., and Vale, R. D. (1997). The directional preference of kinesin motors is specified by an element outside of the motor catalytic domain. Cell *90*, 959-966.

Chu, H. M., Yun, M., Anderson, D. E., Sage, H., Park, H. W., and Endow, S. A. (2005). Kar3 interaction with Cik1 alters motor structure and function. Embo J.

Cole, D. G., Chinn, S. W., Wedaman, K. P., Hall, K., Vuong, T., and Scholey, J. M. (1993). Novel heterotrimeric kinesin-related protein purified from sea urchin eggs. Nature *366*, 268-270.

Cole, D. G., Diener, D. R., Himelblau, A. L., Beech, P. L., Fuster, J. C., and Rosenbaum, J. L. (1998). Chlamydomonas kinesin-II-dependent intraflagellar transport (IFT): IFT particles contain proteins required for ciliary assembly in Caenorhabditis elegans sensory neurons. J Cell Biol *141*, 993-1008.

Coy, D. L., Wagenbach, M., and Howard, J. (1999). Kinesin takes one 8-nm step for each ATP that it hydrolyzes. J Biol Chem *274*, 3667-3671.

Crevel, I. M., Lockhart, A., and Cross, R. A. (1996). Weak and strong states of kinesin and ncd. J Mol Biol *257*, 66-76.

Crevel, I. M., Lockhart, A., and Cross, R. A. (1997). Kinetic evidence for low chemical processivity in ncd and Eg5. J Mol Biol *273*, 160-170.

deCastro, M. J., Fondecave, R. M., Clarke, L. A., Schmidt, C. F., and Stewart, R. J. (2000). Working strokes by single molecules of the kinesin-related microtubule motor ncd. Nat Cell Biol *2*, 724-729.

Endow, S. A., Henikoff, S., and Soler-Niedziela, L. (1990). Mediation of meiotic and early mitotic chromosome segregation in Drosophila by a protein related to kinesin. Nature *345*, 81-83.

Endow, S. A., and Higuchi, H. (2000). A mutant of the motor protein kinesin that moves in both directions on microtubules. Nature *406*, 913-916.

Endow, S. A., Kang, S. J., Satterwhite, L. L., Rose, M. D., Skeen, V. P., and Salmon, E. D. (1994). Yeast Kar3 is a minus-end microtubule motor protein that destabilizes microtubules preferentially at the minus ends. Embo J *13*, 2708-2713.

Endow, S. A., and Waligora, K. W. (1998). Determinants of kinesin motor polarity. Science *281*, 1200-1202.

Foster, K. A., Correia, J. J., and Gilbert, S. P. (1998). Equilibrium binding studies of non-claret disjunctional protein (Ncd) reveal cooperative interactions between the motor domains. J Biol Chem *273*, 35307-35318.

Friedman, D. S., and Vale, R. D. (1999). Single-molecule analysis of kinesin motility reveals regulation by the cargo-binding tail domain. Nat Cell Biol *1*, 293-297.

Goshima, G., and Vale, R. D. (2003). The roles of microtubule-based motor proteins in mitosis: comprehensive RNAi analysis in the Drosophila S2 cell line. J Cell Biol *162*, 1003-1016.

Gunawardena, S., and Goldstein, L. S. (2004). Cargo-carrying motor vehicles on the neuronal highway: transport pathways and neurodegenerative disease. J Neurobiol *58*, 258-271.

Guzik, B. W., and Goldstein, L. S. (2004). Microtubule-dependent transport in neurons: steps towards an understanding of regulation, function and dysfunction. Curr Opin Cell Biol *16*, 443-450.

Hackney, D. D. (1994). Evidence for alternating head catalysis by kinesin during microtubule-stimulated ATP hydrolysis. Proc Natl Acad Sci U S A *91*, 6865-6869.

Hackney, D. D. (1995). Highly processive microtubule-stimulated ATP hydrolysis by dimeric kinesin head domains. Nature *377*, 448-450.

Hackney, D. D., Levitt, J. D., and Suhan, J. (1992). Kinesin undergoes a 9 S to 6 S conformational transition. J Biol Chem *267*, 8696-8701.

Heald, R. (2000). Motor function in the mitotic spindle. Cell *102*, 399-402.

Hirokawa, N., and Takemura, R. (2004). Kinesin superfamily proteins and their various functions and dynamics. Exp Cell Res *301*, 50-59.

Hirose, K., Cross, R. A., and Amos, L. A. (1998). Nucleotide-dependent structural changes in dimeric NCD molecules complexed to microtubules. J Mol Biol *278*, 389-400.

Hirose, K., Lockhart, A., Cross, R. A., and Amos, L. A. (1996). Three-dimensional cryoelectron microscopy of dimeric kinesin and ncd motor domains on microtubules. Proc Natl Acad Sci U S A *93*, 9539-9544.

Howard, J., Hudspeth, A. J., and Vale, R. D. (1989). Movement of microtubules by single kinesin molecules. Nature *342*, 154-158.

Hunter, A. W., Caplow, M., Coy, D. L., Hancock, W. O., Diez, S., Wordeman, L., and Howard, J. (2003). The kinesin-related protein MCAK is a microtubule depolymerase that forms an ATP-hydrolyzing complex at microtubule ends. Mol Cell *11*, 445-457.

Kamal, A., and Goldstein, L. S. (2002). Principles of cargo attachment to cytoplasmic motor proteins. Curr Opin Cell Biol *14*, 63-68.

Karabay, A., and Walker, R. A. (1999). Identification of microtubule binding sites in the Ncd tail domain. Biochemistry *38*, 1838-1849.

King, S. J., and Schroer, T. A. (2000). Dynactin increases the processivity of the cytoplasmic dynein motor. Nat Cell Biol *2*, 20-24.

Klopfenstein, D. R., Tomishige, M., Stuurman, N., and Vale, R. D. (2002). Role of phosphatidylinositol(4,5)bisphosphate organization in membrane transport by the Unc104 kinesin motor. Cell *109*, 347-358.

Kozielski, F., De Bonis, S., Burmeister, W. P., Cohen-Addad, C., and Wade, R. H. (1999). The crystal structure of the minus-end-directed microtubule motor protein ncd reveals variable dimer conformations. Structure Fold Des *7*, 1407-1416.

Kozielski, F., Sack, S., Marx, A., Thormahlen, M., Schonbrunn, E., Biou, V., Thompson, A., Mandelkow, E. M., and Mandelkow, E. (1997). The crystal structure of dimeric kinesin and implications for microtubule-dependent motility. Cell *91*, 985-994.

Lockhart, A., and Cross, R. A. (1994). Origins of reversed directionality in the ncd molecular motor. Embo J *13*, 751-757.

Lupas, A., Van Dyke, M., and Stock, J. (1991). Predicting coiled coils from protein sequences. Science *252*, 1162-1164.

Ma, Y. Z., and Taylor, E. W. (1997). Interacting head mechanism of microtubule-kinesin ATPase. J Biol Chem *272*, 724-730.

Mallik, R., Carter, B. C., Lex, S. A., King, S. J., and Gross, S. P. (2004). Cytoplasmic dynein functions as a gear in response to load. Nature *427*, 649-652.

Mandelkow, E., and Mandelkow, E. M. (2002). Kinesin motors and disease. Trends Cell Biol *12*, 585-591.

McDonald, H. B., Stewart, R. J., and Goldstein, L. S. (1990). The kinesin-like ncd protein of Drosophila is a minus end-directed microtubule motor. Cell *63*, 1159-1165.

Mehta, A. D., Rock, R. S., Rief, M., Spudich, J. A., Mooseker, M. S., and Cheney, R. E. (1999). Myosin-V is a processive actin-based motor. Nature *400*, 590-593.

Menetrey, J., Bahloul, A., Wells, A. L., Yengo, C. M., Morris, C. A., Sweeney, H. L., and Houdusse, A. (2005). The structure of the myosin VI motor reveals the mechanism of directionality reversal. Nature *435*, 779-785.

Miki, H., Okada, Y., and Hirokawa, N. (2005). Analysis of the kinesin superfamily: insights into structure and function. Trends Cell Biol *15*, 467-476.

Ou, G., Blacque, O. E., Snow, J. J., Leroux, M. R., and Scholey, J. M. (2005a). Functional coordination of intraflagellar transport motors. Nature *436*, 583-587.

Ou, G., Qin, H., Rosenbaum, J. L., and Scholey, J. M. (2005b). The PKD protein qilin undergoes intraflagellar transport. Curr Biol *15*, R410-411.

Park, H., Ramamurthy, B., Travaglia, M., Safer, D., Chen, L. Q., Franzini-Armstrong, C., Selvin, P. R., and Sweeney, H. L. (2006). Full-length myosin VI dimerizes and moves processively along actin filaments upon monomer clustering. Mol Cell *21*, 331-336.

Pechatnikova, E., and Taylor, E. W. (1997). Kinetic mechanism of monomeric non-claret disjunctional protein (Ncd) ATPase. J Biol Chem *272*, 30735-30740.

Pechatnikova, E., and Taylor, E. W. (1999). Kinetics processivity and the direction of motion of Ncd. Biophys J *77*, 1003-1016.

Perkins, L. A., Hedgecock, E. M., Thomson, J. N., and Culotti, J. G. (1986). Mutant sensory cilia in the nematode Caenorhabditis elegans. Dev Biol *117*, 456-487.

Pierce, D. W., Hom-Booher, N., Otsuka, A. J., and Vale, R. D. (1999). Single-molecule behavior of monomeric and heteromeric kinesins. Biochemistry *38*, 5412-5421.

Reddy, A. S., and Day, I. S. (2001). Kinesins in the Arabidopsis genome: a comparative analysis among eukaryotes. BMC Genomics *2*, 2.

Rice, S., Lin, A. W., Safer, D., Hart, C. L., Naber, N., Carragher, B. O., Cain, S. M., Pechatnikova, E., Wilson-Kubalek, E. M., Whittaker, M., *et al.* (1999). A structural change in the kinesin motor protein that drives motility. Nature *402*, 778-784.

Romberg, L., Pierce, D. W., and Vale, R. D. (1998). Role of the kinesin neck region in processive microtubule-based motility. J Cell Biol *140*, 1407-1416.

Romberg, L., and Vale, R. D. (1993). Chemomechanical cycle of kinesin differs from that of myosin. Nature *361*, 168-170.

Rosenfeld, S. S., Fordyce, P. M., Jefferson, G. M., King, P. H., and Block, S. M. (2003). Stepping and stretching. How kinesin uses internal strain to walk processively. J Biol Chem *278*, 18550-18556.

Rosenfeld, S. S., Xing, J., Jefferson, G. M., and King, P. H. (2005). Docking and rolling, a model of how the mitotic motor Eg5 works. J Biol Chem *280*, 35684-35695.

Sablin, E. P., Case, R. B., Dai, S. C., Hart, C. L., Ruby, A., Vale, R. D., and Fletterick, R. J. (1998). Direction determination in the minus-end-directed kinesin motor ncd. Nature *395*, 813-816.

Sablin, E. P., Kull, F. J., Cooke, R., Vale, R. D., and Fletterick, R. J. (1996). Crystal structure of the motor domain of the kinesin-related motor ncd. Nature *380*, 555-559.

Schnitzer, M. J., and Block, S. M. (1997). Kinesin hydrolyses one ATP per 8-nm step. Nature *388*, 386-390.

Scholey, J. M. (2003). Intraflagellar transport. Annu Rev Cell Dev Biol *19*, 423-443.

Scholey, J. M., Ou, G., Snow, J., and Gunnarson, A. (2004). Intraflagellar transport motors in Caenorhabditis elegans neurons. Biochem Soc Trans *32*, 682-684.

Shakir, M. A., Fukushige, T., Yasuda, H., Miwa, J., and Siddiqui, S. S. (1993). C. elegans osm-3 gene mediating osmotic avoidance behaviour encodes a kinesin-like protein. Neuroreport *4*, 891-894.

Sharp, D. J., McDonald, K. L., Brown, H. M., Matthies, H. J., Walczak, C., Vale, R. D., Mitchison, T. J., and Scholey, J. M. (1999a). The bipolar kinesin, KLP61F, cross-links microtubules within interpolar microtubule bundles of Drosophila embryonic mitotic spindles. J Cell Biol *144*, 125-138.

Sharp, D. J., Rogers, G. C., and Scholey, J. M. (2000). Microtubule motors in mitosis. Nature *407*, 41-47.

Sharp, D. J., Yu, K. R., Sisson, J. C., Sullivan, W., and Scholey, J. M. (1999b). Antagonistic microtubule-sliding motors position mitotic centrosomes in Drosophila early embryos. Nat Cell Biol *1*, 51-54.

Signor, D., Wedaman, K. P., Rose, L. S., and Scholey, J. M. (1999). Two heteromeric kinesin complexes in chemosensory neurons and sensory cilia of Caenorhabditis elegans. Mol Biol Cell *10*, 345-360.

Snow, J. J., Ou, G., Gunnarson, A. L., Walker, M. R., Zhou, H. M., Brust-Mascher, I., and Scholey, J. M. (2004). Two anterograde intraflagellar transport motors cooperate to build sensory cilia on C. elegans neurons. Nat Cell Biol *6*, 1109-1113.

Sosa, H., Dias, D. P., Hoenger, A., Whittaker, M., Wilson-Kubalek, E., Sablin, E., Fletterick, R. J., Vale, R. D., and Milligan, R. A. (1997). A model for the microtubule-Ncd motor protein complex obtained by cryo-electron microscopy and image analysis. Cell *90*, 217-224.

Sproul, L. R., Anderson, D. J., Mackey, A. T., Saunders, W. S., and Gilbert, S. P. (2005). Cik1 targets the minus-end Kinesin depolymerase kar3 to microtubule plus ends. Curr Biol *15*, 1420-1427.

Stewart, R. J., Thaler, J. P., and Goldstein, L. S. (1993). Direction of microtubule movement is an intrinsic property of the motor domains of kinesin heavy chain and Drosophila ncd protein. Proc Natl Acad Sci U S A *90*, 5209-5213.

Suzuki, Y., Yasunaga, T., Ohkura, R., Wakabayashi, T., and Sutoh, K. (1998). Swing of the lever arm of a myosin motor at the isomerization and phosphate-release steps. Nature *396*, 380-383.

Svoboda, K., and Block, S. M. (1994). Force and velocity measured for single kinesin molecules. Cell *77*, 773-784.

Thorn, K. S., Ubersax, J. A., and Vale, R. D. (2000). Engineering the processive run length of the kinesin motor. J Cell Biol *151*, 1093-1100.

Tomishige, M., Klopfenstein, D. R., and Vale, R. D. (2002). Conversion of Unc104/KIF1A kinesin into a processive motor after dimerization. Science *297*, 2263-2267.

Tomishige, M., and Vale, R. D. (2000). Controlling kinesin by reversible disulfide cross-linking. Identifying the motility-producing conformational change. J Cell Biol *151*, 1081-1092.

Uyeda, T. Q., Abramson, P. D., and Spudich, J. A. (1996). The neck region of the myosin motor domain acts as a lever arm to generate movement. Proc Natl Acad Sci U S A *93*, 4459-4464.

Vale, R. D. (2003). The molecular motor toolbox for intracellular transport. Cell *112*, 467-480.

Vale, R. D., and Milligan, R. A. (2000). The way things move: looking under the hood of molecular motor proteins. Science *288*, 88-95.

Valentine, M. T., Fordyce, P. M., Krzysiak, T. C., Gilbert, S. P., and Block, S. M. (2006). Individual dimers of the mitotic kinesin motor Eg5 step processively and support substantial loads in vitro. Nat Cell Biol *8*, 470-476.

Wedaman, K. P., Meyer, D. W., Rashid, D. J., Cole, D. G., and Scholey, J. M. (1996). Sequence and submolecular localization of the 115-kD accessory subunit of the heterotrimeric kinesin-II (KRP85/95) complex. J Cell Biol *132*, 371-380.

Wendt, T., Karabay, A., Krebs, A., Gross, H., Walker, R., and Hoenger, A. (2003). A structural analysis of the interaction between ncd tail and tubulin protofilaments. J Mol Biol *333*, 541-552.

Wendt, T. G., Volkmann, N., Skiniotis, G., Goldie, K. N., Muller, J., Mandelkow, E., and Hoenger, A. (2002). Microscopic evidence for a minus-end-directed power stroke in the kinesin motor ncd. Embo J *21*, 5969-5978.

Woehlke, G., Ruby, A. K., Hart, C. L., Ly, B., Hom-Booher, N., and Vale, R. D. (1997). Microtubule interaction site of the kinesin motor. Cell *90*, 207-216.

Wordeman, L., and Mitchison, T. J. (1995). Identification and partial characterization of mitotic centromere-associated kinesin, a kinesin-related protein that associates with centromeres during mitosis. J Cell Biol *128*, 95-104.

Yang, Y., Kovacs, M., Sakamoto, T., Zhang, F., Kiehart, D. P., and Sellers, J. R. (2006). Dimerized Drosophila myosin VIIa: a processive motor. Proc Natl Acad Sci U S A *103*, 5746-5751.

Yildiz, A., Tomishige, M., Vale, R. D., and Selvin, P. R. (2004). Kinesin walks hand-over-hand. Science *303*, 676-678.

Yun, M., Bronner, C. E., Park, C. G., Cha, S. S., Park, H. W., and Endow, S. A. (2003). Rotation of the stalk/neck and one head in a new crystal structure of the kinesin motor protein, Ncd. Embo J *22*, 5382-5389.

Zhang, Y., and Hancock, W. O. (2004). The two motor domains of KIF3A/B coordinate for processive motility and move at different speeds. Biophys J *87*, 1795-1804.